Landslides (2014) 11:441–461
DOI 10.1007/s10346-013-0404-6
Received: 19 December 2012
Accepted: 12 April 2013
Published online: 3 May 2013

Chong Xu · Xiwei Xu · Xin Yao · Fuchu Dai

Three (nearly) complete inventories of landslides triggered by the May 12, 2008 Wenchuan Mw 7.9 earthquake of China and their spatial distribution statistical analysis

Abstract The May 12, 2008 Wenchuan earthquake of China (Mw 7.9 or Ms 8.0) triggered hundreds of thousands of landslides. Mapping such a large number of landslides is a major task, considering the large size of the affected area and the availability of pre- and post-earthquake remote sensing images. This paper compares three (nearly) complete landslide inventories that were compiled from visual image interpretation. The three inventories differ in the manner in which the landslides are represented, either as polygons, centroid points, or top points. Landslides in the three inventories use one-to-one correspondence. Each of the three inventories includes a large proportion of the 197,481 landslides triggered by the earthquake. These landslides were delineated as individual solid polygons and points using visual interpretation of high-resolution aerial photographs and satellite images acquired following the earthquake and verified by selected field checking throughout a broad area of approximately 110,000km^2. These landslides cover a total area of approximately 1,160km^2. Based on the inventories of landslide polygons and landslide centroid points, two types of density maps were constructed. Correlations of landslide occurrence with seismic, geologic, and topographic parameters were analyzed using the three landslide inventories. Statistical analysis of their spatial distribution was performed using both the landslide area percentage (LAP), defined as the percentage of the area affected by the landslides and the landslide number density (LND), defined as the number of landslides per square kilometer. There are two types of LNDs: the LND-centroid (based on the centroid point of the landslide) and the LND-top (based on the top point of the landslide). We used the three indexes to determine how the occurrence of the landslides correlates with elevation, slope angle, slope aspect, slope position, slope curvature, lithology, distance from the epicenter, seismic intensity, distance from the Yingxiu-Beichuan surface fault rupture, peak ground acceleration (PGA), and coseismic surface displacements (including horizontal, vertical, and total displacements). Both the LAP and the two types of LND values were observed to have continuous positive or negative correlations with the slope angle, slope curvature, distance from the epicenter and from the Yingxiu-Beichuan surface fault rupture, seismic intensity, and coseismic surface displacement. In addition, the highest values of the LAP and LND values appear at ranges from 1,200 to 3,000m in elevation. Moreover, the landslides have preferred orientations, dominated by the eastern, southeastern, and southern directions. In addition, the sandstone, siltstone (Z), and granitic rocks experienced more concentrated landslides. No obvious correlations were observed between the LAP and LND values and slope position. Finally, we studied the orders of eight earthquake-triggered landslide impact factor effect on landslide occurrence.

Highlights The 197,481 landslides triggered by the 2008 Wenchuan earthquake were delineated.

Three landslide inventories were constructed: polygon, centroid, and top point inventories.

The landslides were spatially analyzed with topographic, lithology, and seismic parameters.

Keywords The 2008 Wenchuan earthquake · Landslides · Inventory · Statistical analysis · Spatial distribution · Landslide area percentage · Landslide number density

Introduction

The landslides triggered by the 2008 Wenchuan earthquake have received much attention in recent years due to the size of the event and the resulting tragic loss of life and economic devastation. Correlating landslide occurrence with controlling parameters is important for understanding the spatial distribution of earthquake-triggered landslides. It is important to understand what areas are most likely to experience landsliding in future earthquakes. A detailed, comprehensive, and accurate earthquake-triggered landslide inventory is an essential part of improving the understanding of seismic landslide hazard analysis (e.g., Keefer 2002; Harp et al. 2011a; Guzzetti et al. 2012). After the 2008 Wenchuan earthquake, some landslide inventories were compiled (e.g., Dai et al. 2011; Xu et al. 2009a; Gorum et al. 2011; Huang and Li 2009; Parker et al. 2011; Chigira et al. 2010; Yin et al. 2010a; Qi et al. 2010; Li et al. 2009; Han et al. 2009; Di et al. 2010; Chen et al. 2009; Ren and Lin 2010; Zhang et al. 2010), and correlations of landslide occurrence with geologic and geomorphologic conditions as well as seismic parameters were constructed. However, almost all of the inventories are either incomplete or only record landslide locations; no landslide inventories are comprehensive considering the following seismic landslide mapping criteria: (1) coverage of the entire area affected by landslides, (2) inclusion of all landslides down to a small enough scale, and (3) depiction of landslides as polygons rather than points (Harp et al. 2011a). Therefore, in this paper, three (nearly) complete landslide inventories were compiled for a detailed and objective spatial distribution statistical analysis of the landslides triggered by the 2008 Wenchuan earthquake.

Concerning single earthquake events, most studies have focused on compiling landslide inventories, scenario-based analysis, and finding general correlations of landslide occurrence with various landslide-controlling parameters, such as the slope gradient, distance from the earthquake source, geologic units, and slope aspect. The analysis of earthquake-triggered landslide inventories was initiated by Keefer (1984) who performed a statistical analysis

of landslide distributions associated with 40 historical worldwide earthquakes occurring from 1811 to 1980. A database of earthquake-triggered landslide inventories was compiled to cover the period from 1980 to 1997 by Rodriguez et al. (1999), which extends the work of Keefer (1984). However, most of the inventories in this database are incomplete. Keefer (2002) and Harp et al. (2011a) discussed the quality of landslide inventories and the need to represent landslides as individual polygons. One of the first complete landslide inventories was performed for the 17 January 1994 Mw 6.7 Northridge earthquake (Keefer 1984, 2002; Harp et al. 2011a). Examples of earlier earthquake-triggered landslide inventory maps include the one with more than 220 large landslides in the Madrid seismic zone, Tennessee, and Kentucky, which was triggered by the 16 December 1811 New Madrid, Mo., earthquakes (Jibson and Keefer 1989). At least 1,850 landslides were triggered by the 17 June 1929 M 7.7 Murchison earthquake (Pearce and O'Loughlin 1985). Other coseismic landslide inventories for earthquakes that occurred before the 1994 Mw 6.7 Northridge earthquake include the December 26, 1949 M 6.2 and 6.4 Imaichi earthquakes (Morimoto 1950, 1951; Morimoto et al. 1957), the May 31, 1970 M 7.9 Peru earthquake (Plafker et al. 1971), the M 6.7 February 9, 1971 San Fernando earthquake (Morton 1971), the 1976 Guatemala earthquake (Harp et al. 1978, 1981), the 1980 Mammoth Lakes earthquake (Harp et al. 1984), the 1983 Coalinga earthquake (Harp and Keefer 1990), the May 1976 Friuli, Italy M 6.4 earthquake (Govi 1977), the 17 October 1989 Mw 6.9 Loma Prieta earthquake (Keefer 2000), the March 5, 1987 Ecuador earthquake (Tibaldi et al. 1995), and the 23 November 1980 Ms 6.9 Irpinia earthquake (Wasowski et al. 2002).

The first digital inventory map for earthquake-triggered landslides was compiled by Harp and Jibson (1995, 1996). More than 11,000 landslides were registered by the 17 January 1994 Mw 6.7 Northridge earthquake from visual interpretation of aerial photography and select field verification. The most common types of landslides triggered by the earthquake were highly disrupted falls and slides (Jibson and Harp 1994). This landslide inventory was used to assess the correlation between landslides and slope gradient, slope aspect, Arias intensity, and geologic units (Parise and Jibson 2000; Khazai and Sitar 2004; Malamud et al. 2004a; Meunier et al. 2007, 2008; Harp et al. 2011a) as well as the correlations among landslides, earthquakes, and erosion (Malamud et al. 2004b).

The 21 September 1999, Mw 7.5 Chi-chi earthquake in Taiwan resulted in a landslide inventory map that is comprised of 9,272 landslides interpreted from SPOT images (Liao and Lee 2000; Liao et al. 2002). Furthermore, this inventory has also been used extensively to compare various landslide controlling factors with the landslide distribution (Weissel and Stark 2001; Wang et al. 2003; Lin and Tung 2004; Lee et al. 2008; Khazai and Sitar 2004) and geomorphology evolution in a part of the earthquake-affected area (Dadson et al. 2003, 2004, 2005; Hovius et al. 2009, 2011; Harp et al. 2011a; Wasowski et al. 2011). In addition, Wang et al. (2002) reported the numbers of landslides to be approximately 26,000 (Wasowski et al. 2011) when landslides of smaller size are included.

There are several papers on the October 8, 2005 Mw 7.6 Kashmir earthquake-triggered landslides. Das et al. (2007) performed a rapid analysis of earthquake-triggered landslide spatial patterns using satellite data, and the results highlighted a trend in landslide zones in the NW–SE direction, mostly affecting the southeast-facing slopes. Kamp et al. (2008) identified 2,252 landslides triggered by the earthquake and analyzed the correlations between landslides and lithology, faults, slope gradient, slope aspect, elevation, land cover, rivers, and roads. Sato et al. (2007) interpreted 2,424 landslides triggered by the earthquake using SPOT 5 stereo images. The landslide distribution indicated that most of the landslides occurred along the seismogenic fault, concentrated on the hanging wall. Owen et al. (2008) reported that earthquake-triggered landslides concentrated in specific zones were associated with the lithology, tectonic, geomorphology, and topography as well as with human activities.

For the October 23, 2004 Mid-Niigata earthquake-triggered landslides, Yamagishi and Iwahashi (2007) mapped approximately 3,500 landslides triggered by the July 13, 2004 heavy rainfalls and 4,400 landslides triggered by the earthquake. These authors provided a comparison of the distribution of features between these landslides and compared the correlations between landslide spatial distribution and lithology, curvatures, and slope gradient. Chigira and Yagi (2006) mapped approximately 1,000 landslides by field investigation and aerial photograph interpretation and analyzed the geological and geomorphologic characteristics of the landslides. Sato et al. (2005) identified 1,353 individual landslides triggered by the earthquake as single polygons and overlaid the landslides on the earthquake source, and geological and topographical data to determine the characteristics of the landslide distribution triggered by the earthquake. Wang et al. (2007) mapped 1,212 landslides triggered by the earthquake in a selected landslide intensity square area near the epicenter and provided useful insights into the correlations between the earthquake-triggered landslides and the geology, slope gradient, and earthquake shaking.

In addition, Fukuoka et al. (1997) mapped 674 landslides triggered by the 17 January 1995 Hyogo-ken earthquake (Ms 7.2 or Mw 6.9) within an area of approximately 700 km^2. These researchers revealed an attenuation trend between the landslide frequency and distance from the assumed fault rupture zone. Marzorati et al. (2002) mapped approximately 200 landslides triggered by the 26 September 1997 Umbria-Marche earthquake using a set of aerial photographs and field surveys. These authors analyzed the correlation between the landslides and environmental and seismic factors such as the distance from epicenter, peak ground acceleration (PGA), and slope gradient. Other inventories of landslides triggered by earthquakes occurring between the January 17, 1994 Mw 6.7 Northridge earthquake and the 2008 Wenchuan earthquake were also prepared, such as for the July 16, 2007 Mw 6.6 Niigata Chuetsu-Oki earthquake (Collins et al. 2012), the January 21, 2003 Mw 7.6 Tecomán, Mexico earthquake (Keefer et al. 2006), and the 2007 Aysén Fjord earthquake (Sepúlveda et al. 2010).

After the 2008 Wenchuan earthquake, several inventories of coseismic landslides were compiled. These events include the April 14, 2010 Mw 6.9 Yushu earthquake of China, the January 12, 2010 Mw 7.0 Haiti earthquake, the June 14, 2008 Iwate-Miyagi Nairiku earthquake, and the May 11, 2011 Mw 5.1 Lorca, SE Spain earthquake. In total, 282 landslides were triggered by the Yushu earthquake according to a post-earthquake emergency investigation (Yin et al. 2010b). A detailed inventory revealed that 2,036 landslides were delineated from high-resolution aerial photographs and satellite

images, which were verified by selected field checking (Xu et al. 2012a, 2013a). Similarly, some inventories of landslides triggered by the Haiti earthquake were also constructed for coseismic landslide spatial distribution analysis and hazard analysis (Xu et al. 2012b; Xu and Xu 2012a; Gorum et al. 2013; Harp et al. 2011b). The June 14, 2008 Iwate-Miyagi Nairiku earthquake triggered at least 4,161 landslides (Yagi et al. 2009), and the May 11, 2011 Mw 5.1 Lorca, SE Spain earthquake triggered more than 250 landslides (Alfaro et al. 2012).

In the following text, three (nearly) complete inventories of landslides triggered by the 2008 Wenchuan earthquake will be introduced in detail. The spatial distribution of the landslides triggered by the earthquake was obtained by correlating the landslide area percentage (LAP), landslide number density (LND)-centroid, and LND-top with the impact factors that control earthquake-triggered landslide occurrence. These factors include the elevation, slope angle, slope aspect, slope curvature, slope position, lithology, distance from epicenter, distance from the Yingxiu-Beichuan surface fault rupture, PGA, seismic intensity, and coseismic surface displacement (horizontal, vertical, and total displacements). Furthermore, the effects of eight impact factors on landslide occurrence were compared using a bivariate statistical method.

Tectonic setting and the 2008 Wenchuan earthquake

At 14:28 (Beijing Time) on May 12, 2008, a catastrophic earthquake with Mw 7.9 (or Mw 8.0) struck Wenchuan County in Sichuan Province, China. This earthquake is known as the Wenchuan earthquake, as its epicenter was located in the administrative region of Wenchuan County. The epicenter, approximately 80 km west-northwest of Chengdu, the capital of Sichuan Province, is located at 31.021°N and 103.367°E with a focal depth of 14 km. As of February 10, 2010, 311 major aftershocks with magnitudes of Ms≥4.0 have been recorded, with the strongest measured Ms 6.4 occurring on May 25, 2008. According to the Government of China, as of September 25, 2008, 69,227 people have been confirmed dead, with 17,923 missing, and 374,643 injured in this earthquake, which also destroyed innumerable infrastructures and houses.

The Ms 8.0 Wenchuan earthquake occurred in the Longmenshan mountain range, an area that is deforming because of the collision between the Indian plate and the Eurasian plate. The Indian plate has been moving northward, resulting in an uplift of the Tibetan Plateau. The deformation has also resulted in the extrusion of crustal material from the high Tibetan Plateau in the west against the strong crustal material of the Sichuan Basin, which is a part of the Yangtze block (Xu et al. 2008a). The Ms 8.0 Wenchuan earthquake ruptured two large thrust faults along the Longmenshan thrust belt at the eastern margin of the Tibetan Plateau. This earthquake produced a 240-km-long surface rupture zone along the Yingxiu-Beichuan fault characterized by right-lateral oblique faulting and a 72-km-long surface rupture zone along the Guanxian-Jiangyou fault characterized by dip-slip reverse faulting (Xu et al. 2008b; Xu et al. 2009b, 2009c). In addition, a 6-km-long NW-trending surface rupture with reverse and left-slip components was also observed (Fig. 1).

Mapping of landslides triggered by the earthquake

Figure 2 shows the spatial coverage of the remote sensing images collected for landslide visual interpretation. We collected 86 images pre- and post-earthquake: 63 images representing the pre-earthquake and 23 images associated with the post-earthquake. The post-earthquake images include aerial photographs acquired at 1-m, 2-m, 2.4-m, and 5-m resolutions, SPOT 5 with 2.5-m resolution, CBERS02B with 19.5-m resolution, IKONOS with 1-m resolution, ASTER with 15-m resolution, IRS-P5 with 2.5-m resolution, QuickBird with 0.6- and 2.4-m resolutions, and ALOS with 2.5-m resolution (Table 1). A few hundred landslides occurred in areas lacking clear images, and these were delineated from the visual interpretation of images post-earthquake on the Google Earth platform. The pre-earthquake images consisted of SPOT 5 with 2.5-m resolution covering some parts of the approximate distribution area of the landslides and ETM+ with 15-m resolution throughout the entire approximate landslide area (Table 1).

A detailed and accurate landslide inventory is an essential component of seismic landslide hazard analyses (e.g., Xu et al. 2012c, 2012d, 2012e, 2012f, 2013b, 2013c; Xu and Xu 2012c) and spatial distribution statistical analyses (e.g., Xu and Xu 2012b, 2013; Dai et al. 2011; Gorum et al. 2011, 2013; Harp et al. 2011a). Harp et al. (2011a) considered an ideal inventory as one covering the entire area affected by an earthquake, including all the landslides that are detectable down to a size of 1–5 m in length, with the landslides being accurately located and mapped as polygons depicting their true shapes. Such mapped landslide distributions can then be used to perform seismic landslide hazard analysis and other quantitative analyses.

Because of the large area throughout which the Wenchuan earthquake triggered landslides, it is impossible to perform detailed field mapping on every landslide. Instead, the location and boundary of each landslide was delineated by computer screen-based visual interpretation of high-resolution color aerial photographs and satellite remote sensing images, and some landslides were verified by field checking. Due to the high resolution of the true color aerial photographs and satellite remote sensing images, almost all the Wenchuan earthquake-triggered landslides, including the small slope failures, were detected. A spatial distribution map of the earthquake-triggered landslides was prepared in a GIS platform. Up to 197,481 landslides triggered by the earthquake were delineated as individual solid polygons. Furthermore, two types of landslide point inventories were constructed, including landslide centroid points similar to Dai et al. (2011) and landslide top points similar to Qi et al. (2010) and Gorum et al. (2011). Therefore, we compiled three (nearly) complete inventories of landslides triggered by the 2008 Wenchuan earthquake on a GIS platform. As demonstrated in Fig. 1, the results indicate that the earthquake triggered 197,481 landslides throughout an approximately limited area of more than 110,000 km^2. The total surface area of these landslides was approximately 1,160 km^2. According to the empirical relationship between the total area affected by landslides and the Richter earthquake magnitude (Keefer 1984; Rodriguez et al. 1999), an earthquake in Ms 8.0 corresponds to approximately 100,000 km^2 of the upper limit landslide-affected area value. Therefore, the 2008 Ms 8.0 Wenchuan earthquake was slightly beyond the upper band of this prediction.

In the approximately limited area but far away from the Yingxiu-Beichuan fault, there are a few landslides and a lack of high-resolution satellite images. The landslides that occurred in these areas were too small and rare to identify objectively. Therefore, we selected a smaller area than the approximate limited area of the landslides around the coseismic surface fault ruptures as the study area (Fig. 2). The study area covers approximately 44,031 km^2. In total, 196,007 landslides, with a total area of 1,150.622 km^2, occurred in the study area. The study area ranges from 452.9 to 6,245.4 m in elevation over an area of approximately 44,031 km^2. The natural

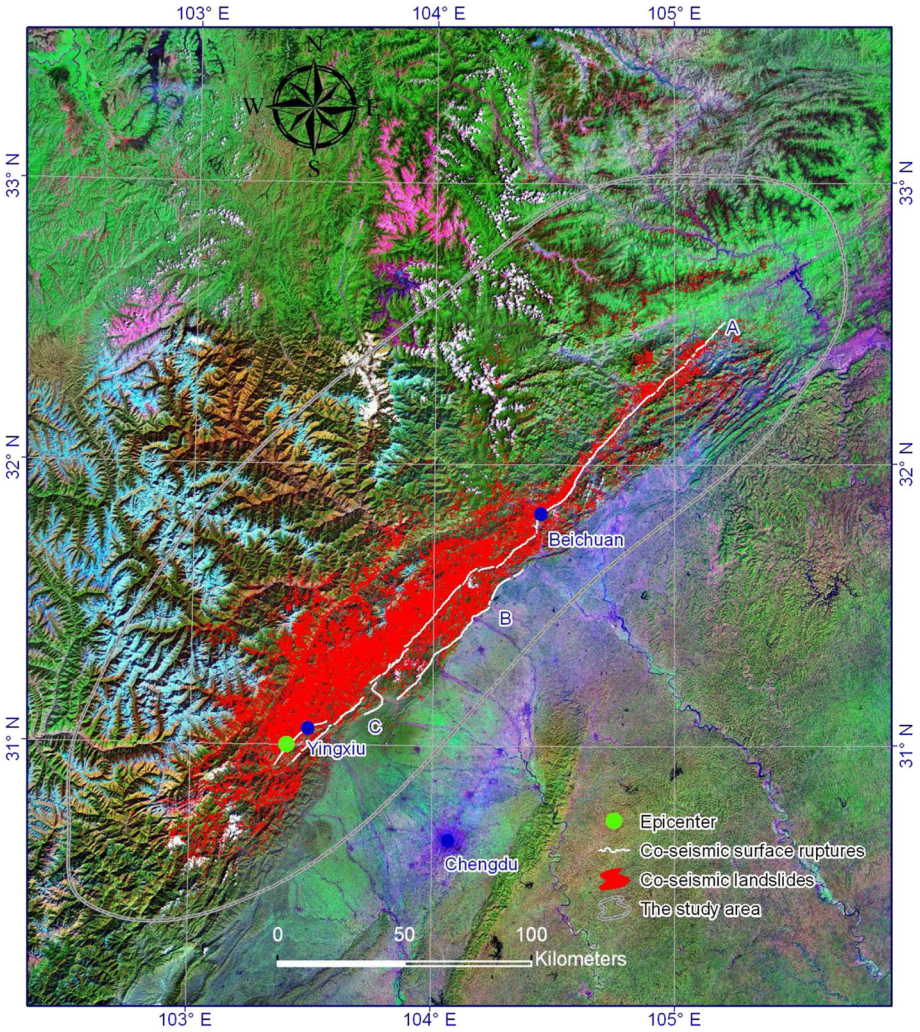

Fig. 1 Distribution of coseismic surface ruptures (*white lines*) and earthquake-triggered landslides (*red polygons*) triggered by the 2008 Wenchuan earthquake. *A* the Yingxiu-Beichuan coseismic surface rupture, *B* the Guanxian-Jiangyou coseismic surface rupture, *C* the Xiaoyudong coseismic surface rupture

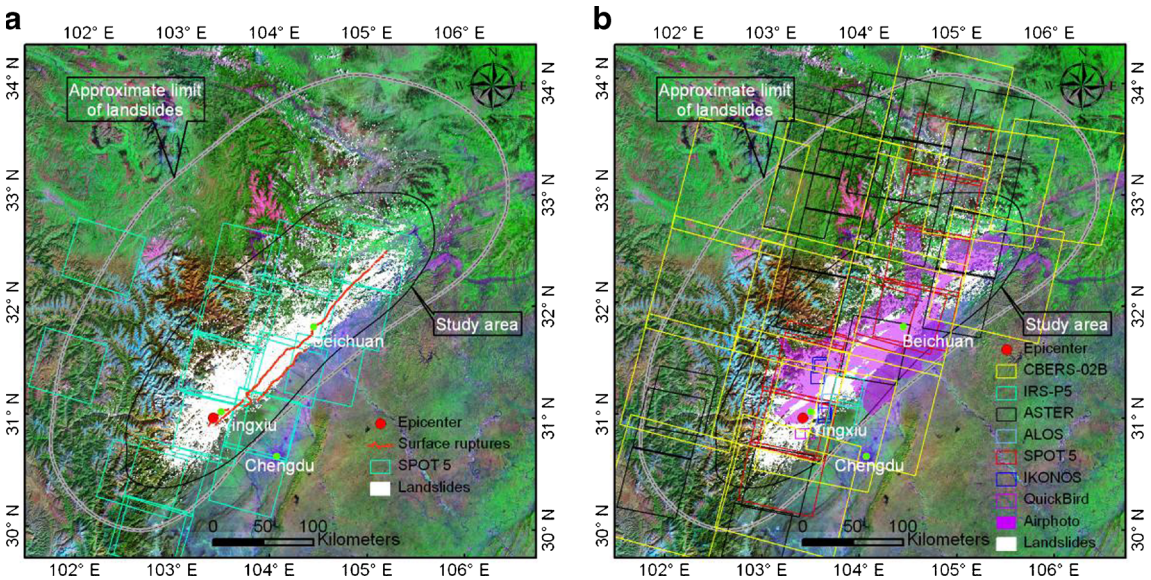

Fig. 2 Pre- and post-earthquake remote sensing image coverage. **a** Pre-earthquake; **b** post-earthquake

Table 1 Remote sensing images data index table

ID	Sensor	Acquisition date	Resolution (m)	Production ID or name
Post-earthquake				
1	Airphoto	2008-05	1, 2, 5	
2	Airphoto	2008-06-13	2.4	
3	SPOT5	2008-05-15	2.5	Missing
4	SPOT5	2008-05-15	2.5	Missing
5	SPOT5	2008-05-15	2.5	Missing
6	SPOT5	2008-05-16	2.5	Missing
7	SPOT5	2008-05-16	2.5	Missing
8	SPOT5	2008-05-16	2.5	Missing
9	SPOT5	2008-05-16	2.5	Missing
10	SPOT5	2008-06-04	2.5	Fusion-261286-080604
11	SPOT5	2009-06-03	2.5	260286200906032012050800717
12	SPOT5	2009-05-20	2.5	259288200905202012050714100
13	SPOT5	2009-05-20	2.5	259287200905202012050714041
14	SPOT5	2009-05-20	2.5	Missing
15	CBERS02B	2008-05-16	19.5	876411
16	CBERS02B	2009-09-21	19.5	949728
17	CBERS02B	2010-01-24	19.5	1103161
18	CBERS02B	2008-11-10	19.5	611641
19	CBERS02B	2008-06-27	19.5	430088
20	CBERS02B	2008-06-27	19.5	430089
21	CBERS02B	2008-06-27	19.5	430090
22	CBERS02B	2008-06-27	19.5	444597
23	CBERS02B	2008-11-27	19.5	635012
24	CBERS02B	2009-02-13	19.5	733872
25	CBERS02B	2009-02-10	19.5	208424
26	CBERS02B	2008-09-04	19.5	157592
27	CBERS02B	2009-04-29	19.5	222402
28	CBERS02B	2009-02-10	19.5	379415
29	CBERS02B	2009-02-10	19.5	208423
30	CBERS02B	2008-12-23	19.5	195239
31	IKONOS	2008-07-01	1	2008070104115830000011619801
32	IKONOS	2008-05-23	1	2008052303514730000011605286
33	IKONOS	2008-05-23	1	2008052303513600000011605290
34	IKONOS	2008-06-28	1	2008062804023290000011616350
35	IKONOS	2008-06-28	1	2008062804022210000011616349
36	ASTER	2008-06-01	15	AST14DMO_00306012008035043_20081216080647_17451
37	ASTER	2008-06-01	15	AST14DMO_00306012008035034_20081216080656_17926
38	ASTER	2008-06-01	15	AST14DMO_00306012008035025_20081216080706_17979
39	ASTER	2008-07-10	15	AST14DMO_00307102008035653_20081216080706_17991
40	ASTER	2008-05-23	15	AST14DMO_00305232008035718_20081216080706_17997
41	ASTER	2008-05-16	15	AST14DMO_00305162008035020_20081216080716_18141
42	ASTER	2008-05-16	15	AST14DMO_00305162008035029_20081216080716_18144
43	ASTER	2008-05-16	15	AST14DMO_00305162008035011_20081216080716_18148

Table 1 (continued)

ID	Sensor	Acquisition date	Resolution (m)	Production ID or name
44	ASTER	2008-05-16	15	AST14DMO_00305162008035047_20081216080727_18339
45	ASTER	2008-06-17	15	AST14DMO_00306172008035018_20081216080738_18933
46	ASTER	2008-07-10	15	AST14DMO_00307102008035644_20081216083230_26664
47	ASTER	2008-12-08	15	AST14DMO_00312082008040342_20081216083321_27056
48	ASTER	2008-12-08	15	AST14DMO_00312082008040333_20081216083322_27065
49	ASTER	2008-11-15	15	AST14DMO_00311152008035703_20081216083321_27068
50	ASTER	2008-08-04	15	AST14DMO_00308042008035020_20081216083332_27188
51	ASTER	2008-07-26	15	AST14DMO_00307262008035724_20081216083342_27256
52	ASTER	2008-07-17	15	AST14DMO_00307172008040245_20081216083402_27355
53	ASTER	2008-07-10	15	AST14DMO_00307102008035636_20081216083402_27361
54	ASTER	2008-07-17	15	AST14DMO_00307172008040236_20081216083402_27371
55	ASTER	2008-07-10	15	AST14DMO_00307102008035627_20081216083402_27373
56	ASTER	2008-12-10	15	AST14DMO_00312102008035055_20081216083311_26906
57	IRS-P5	2008-06-03	2.5	200806032902
58	IRS-P5	2008-06-03	2.5	200806032802
59	QuickBird	2008-06-03	0.6	08JUN03041541-S2AS_R05C1-052017323010_01_P001
60	QuickBird	2008-06-03	0.6	08JUN03041541-S2AS_R05C2-052017323010_01_P001
61	QuickBird	2008-09-01	2.4	08SEP01041602-M2AS-052099005020_01_P001
62	ALOS	2008-06-04	2.5	ALPSMB125753025
63	ALOS	2008-06-04	2.5	ALPSMF125752920
Pre-earthquake				
1	SPOT5	2005-02-10	2.5	SPOT5-261-287-20050210-fusion
2	SPOT5	2005-08-15	2.5	SPOT5-260-288-20050815-fusion
3	SPOT5	2005-08-15	2.5	SPOT5-260-289-20050815-fusion
4	SPOT5	2005-11-01	2.5	SPOT5-259-286-20051101-fusion
5	SPOT5	2005-11-11	2.5	SPOT5-258-290-20051111-fusion
6	SPOT5	2006-12-01	2.5	SPOT5-259-287-20061201-fusion
7	SPOT5	2007-09-18	2.5	SPOT5-256-287-20070918-fusion
8	SPOT5	2008-01-05	2.5	SPOT5-258-289-20080105-fusion
9	SPOT5	2008-01-05	2.5	SPOT5-256-285-20080105-fusion
10	SPOT5	2005-05-09	2.5	52592880505090348341B
11	SPOT5	2005-05-09	2.5	52592880505090348341A
12	SPOT5	2005-11-07	2.5	52592870511070345371J
13	SPOT5	2005-12-03	2.5	52602880512030345112J
14	SPOT5	2006-01-28	2.5	52592880601280408441A
15	SPOT5	2006-08-09	2.5	52582900608090358051A
16	SPOT5	2006-09-05	2.5	52622840609050338001J
17	SPOT5	2006-11-10	2.5	52602850611100408531J
18	SPOT5	2006-11-10	2.5	52602860611100409021J
19	SPOT5	2007-03-20	2.5	52592860703200408062J
20	SPOT5	2007-03-21	2.5	52622860703210348471J
21	SPOT5	2007-05-06	2.5	52602870705060403402J
22	SPOT5	2007-12-06	2.5	52592850712060345201A
23	ETM+[a]	1999–2003	15	N-48-30, throughout the study area

[a] http://datamirror.csdb.cn/mosaicMetaData.lan?mosaicId=N-48-30

slopes in this area are steep, with an average slope angle of 29.2°. In the study area, as shown in Fig. 1, 196,007 landslides, with a total area of 1,150.622 km^2, were triggered by the 2008 Wenchuan earthquake. LAP=1,150.622 km^2 / 44,031.130 km^2×100 %=2.613 %, and LND=196,007 landslides / 44,031.130 km^2=4.452 landslides/km^2. The LAP and LND of the study area are 2.613 % and 4.452 landslides/km^2, respectively. These landslides are concentrated along the coseismic surface fault rupture, and most of the landslides occurred on the hanging wall.

Landslide size and landslide density maps

Landslide size

The relationship of the cumulative landslide number and the landslide area related to the 2008 Wenchuan earthquake can be represented as the logarithm of the number N of landslides exceeding a given area A and is linearly related to the area as described in Formula 1:

$$\lg N(A) = \mathrm{a} + \mathrm{bA} \quad (1)$$

where $N(A)$ represents the cumulative number of landslides which area is larger than or equal to A, and a and b are constants. As A is measured on a logarithmic scale, this relationship is a straight line on a "lg to lg" scale. In Fig. 3, the cumulative number of landslides is plotted as a function of area. Landslides with areas between 10,000 and 1,000,000 m^2 are defined by the equation $lg\,N = -2.0745A + 13$, with R^2=0.9931. For small areas, the curve bends toward the horizontal, as small landslides would overlap with large landslides, or perhaps, it is more difficult to obtain a detailed sample for small landslides.

Landslide density maps

Figure 4 presents the landslide area and LND grid cell maps related to the Wenchuan earthquake. The landslide area and number density (centroid) maps were produced in 1 km×1 km calculation windows for the study area. Figure 4a indicates that the maximum landside density of LAP is 100 %, and Fig. 4b indicates that the largest LND value is 281 landslides/km^2, demonstrating a dense landslide distribution. This figure also reveals that the landslides were primarily concentrated along the Yingxiu-Beichuan surface fault rupture, and most of the landslides occurred on the hanging wall. The highest landslide density area appears in areas near the Yingxiu-Beichuan fault on the hanging wall of the southwest segment (from Yingxiu Town to Beichuan County) of the Yingxiu-Beichuan fault.

Furthermore, correlations between the area distribution and LAP and LND were also constructed. Table 2 provides detailed data on the classes of LAP and LND (centroid) and the area distribution. Figure 5 presents the correlation curves of LAP and LND (centroid) with area distribution. According to Fig. 5a, the area–LAP relationship for the landslides triggered by the Wenchuan earthquake can be represented by $y=61918e^{-0.9574x}$, R^2=0.9725, where y is the area and x is the LAP value. For the LND values (Fig. 5b), there is no data for the ranks of 240–270 (class 10); thus, the mathematical relationship is not obvious. However, we observe that there is a power relationship between the area, and the LAP and LND (Fig. 5b, between classes 1 and 9) values.

Spatial analysis of landslides with controlling parameters

Multivariate statistical methods (e.g., logistic regression, artificial neural network, and support vector machine) are time-consuming and require complex calculations. These methods are not suitable for large areas such as the 2008 Wenchuan earthquake-triggered landslide affected area. Therefore, the bivariate statistics method was selected in this study. However, multivariate statistical methods are more advanced than the bivariate statistical method for factors that are conditionally independent of one another (Xu et al. 2013b). The Wenchuan earthquake provides a good opportunity to study the distribution and effects of landslides triggered by earthquakes on a thrust-strike fault.

Landslide occurrence in an earthquake-struck area is a function of various internal and external dynamic impact factors (Dai et al. 2011), such as slope angle, slope aspect, lithology, distance from the earthquake source, PGA, and coseismic surface displacement. The following correlation analysis of the landslide distribution was performed for the 196,007 landslides triggered by the Wenchuan earthquake, using three indexes of one type of LAP and two types of LND (LND-centroid and LND-top). In the LND analysis, the centroid of the landslides was used to represent the corresponding landslides. These values were extracted from the

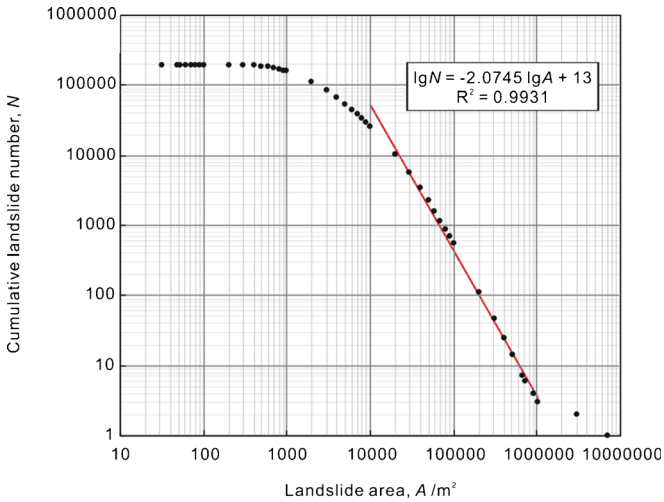

Fig. 3 Curve depicting correlation between the cumulative landslide number and the landslide area

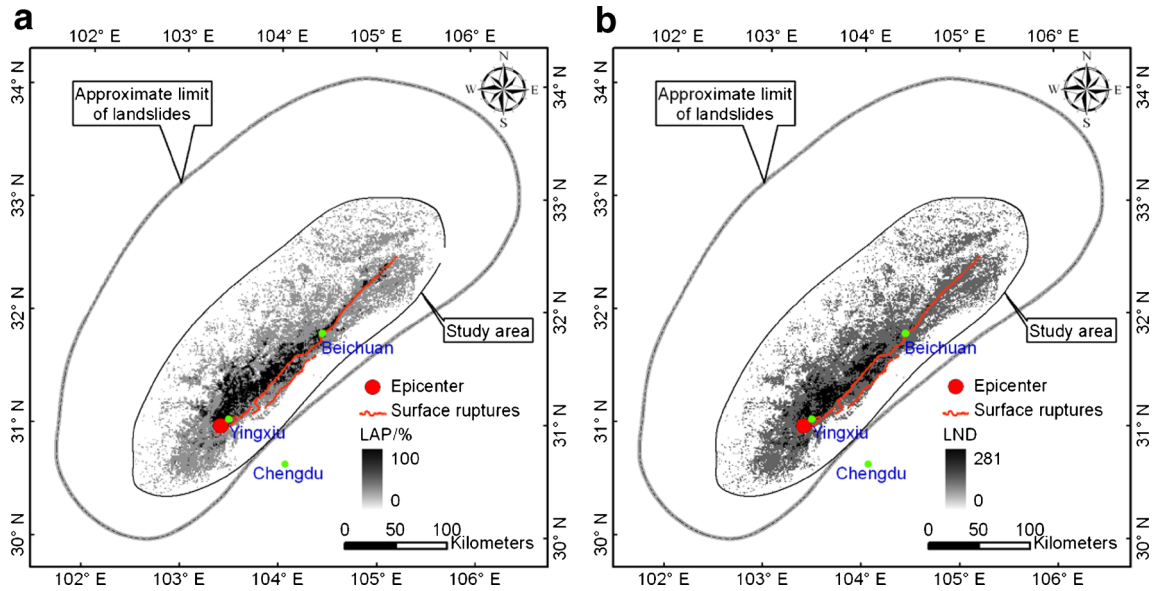

Fig. 4 Density maps of LAP and LND. **a** LAP density map; **b** LND density map. The coseismic surface ruptures were also shown in Fig. 1

landslide polygons using the same procedure as Dai et al. (2011), in which no weight is assigned to account for differences in landslide volumes. Furthermore, another inventory of landslide points, identified by the top position of the landslide scar, similar to the procedure used by Qi et al. (2010) and Gorum et al. (2011), is also plotted for further LND analysis.

The analysis was performed using the digital geological map compiled from 1:200,000 scale standard geological maps (from China Geological Survey Bureau) and digital topographical maps with a scale of 1:50,000 (from the National Administration of Surveying, Mapping and Geoinformation). The digital elevation model (DEM) has a resolution of 20 m×20 m and is constructed by implementation of 1:50,000 scaled topographical map contour lines, contour points, and drainages using GIS software. Some topographical, geological, and seismic parameters, including elevation, slope angle, slope aspect, slope position, slope curvature, lithology, distance from the epicenter, seismic intensity, distance from the Yingxiu-Beichuan surface fault rupture, PGA, and coseismic surface displacements (horizontal, vertical, and total displacements) were selected for the following landslide spatial analysis.

Correlations with topographical parameters

Five topographical parameters, elevation, slope angle, slope aspect, slope curvature, and slope position, were used for correlation with landslide occurrence. The respective classifications of the five layers are indicated below Figs. 6 and 7. Figure 6a presents the LAP, LND-centroid, and LND-top values in relation to the elevation. Area distributions of the 24 elevation classifications are also presented in Fig. 6a. The highest LAP, LND-centroid, and LND-top values are observed to occur at elevations from 1,200 to 3,000 m (classes 5–13). For a landslide, the elevation of the top point is

Table 2 Area distribution with LAP and LND values

Classes of LAP (%)	Area (km^2)	Classes of LND (landslides/km^2)	Area (km^2)
(1): 0	26,124	(1): 0	26,941
(2): 0–10	14,461	(2): 0–30	15,281
(3): 10–20	1,575	(3): 30–60	1,482
(4): 20–30	858	(4): 60–90	269
(5): 30–40	516	(5): 90–120	39
(6): 40–50	310	(6): 120–150	19
(7): 50–60	128	(7): 150–180	4
(8): 60–70	59	(8): 180–210	4
(9): 70–80	5	(9): 210–240	1
(10): 80–90	3	(10): 240–270	0
(11): 90–100	2	(11): 270–281	1

higher than that of the centroid point. Therefore, compared with the curve of LND-centroid values, the curve of the LND-top values is at higher elevation.

The slope angle, slope aspect, and slope curvature were extracted based on the DEM at 20 m×20 m resolution. The slope angle was reclassified at intervals of 5°. The slope angle is known to have a significant effect on landslide occurrence. Steeper and higher slopes have higher susceptibility for landslide occurrence, even when the slope failure is not triggered by an earthquake. As demonstrated in Fig. 6b, both the LAP and LND values generally increase with the slope angle, but slopes exceeding 35° (classes 8–13) are more susceptible to landsliding. Furthermore, the area distributions of the 13 slope angle classifications are also presented in Fig. 6b. The largest area is distributed from 30 to 40° (classes 7 and 8). In addition, Fig. 6b also demonstrates that the curve of the LND-centroid values has higher slope angle. In other words, the LND-centroid values of those slopes exceeding 40° (classes 9–13) are higher than the LND-top values. This result implies that part of the landslides occurred on the mountain peak. Although the elevation of these locations is higher, the slope angle is relatively low. The highest LAP and LND values are also observed for such slopes exceeding a 60° angle (class 13). The LAP and LND values are as high as 17.871 %, and 15.510 and 13.598 landslides/km^2, respectively, as the slope angle exceeds 60°.

The slope aspect is defined as the direction of the maximum slope of the terrain surface and is related to factors such as exposure to sunlight, drying winds, rainfall (degree of saturation), and discontinuities, which may control landslide occurrence (Yalcin 2008). The slope aspect may also have an effect on landsliding because it is related to factors such as directional PGAs (Dai et al. 2011). In addition, the slope aspect of landslide occurrence is perhaps affected by the slipping orientations of the seismogenic fault. The slope aspect was divided into nine classes for the study, including flat, N, NE, E, SE, S, SW, W, and NW. Area distributions of the nine slope aspect classifications are presented in Fig. 6c. The figure also indicates that the eastern, southeastern, and southern directions (classes 4, 5, and 6) were the preferred orientations of landslide-occurring slopes. The main direction roughly corresponded to the thrust direction of the hanging wall. A significant effect of the direction of the hanging wall thrust movement and the seismic wave propagation was observed.

Slope position could also be a controlling factor of landslide occurrence. Landscapes can be classified into discrete slope positions, including ridge, upper slope, middle slope, flat slope, lower slope, and valley (Weiss 2006). The slope position layer is also extracted from DEM at 20 m×20 m resolution based on the GIS platform. Area distributions of the six slope position classifications are presented in Fig. 6d. Both the LAP and LND values (Fig. 6d) exhibit obscure correlations with slope position. Perhaps the reason for these obscure correlations is that two contradictory parameters, seismic wave amplification and distance from drainages, affect landslide occurrence. The undercutting action of the river may trigger instability of the slopes. Thus, the distance of a landslide from drainages was considered as a controlling factor of earthquake-triggered landslides. The slope position effect on landslide occurrence is based on other factors. Perhaps different basin evolution stages have different slope position effects. Even so, the flat slope class (class 4) occupies the special lowest LAP and LND values.

In terms of the slope curvature, negative curvatures represent concave surfaces, a zero curvature represents a flat surface, and positive curvatures represent convex surfaces (Pradhan et al. 2010). The classifications of slope curvature are presented in Fig. 7. Area distributions of the 12 slope curvature classifications

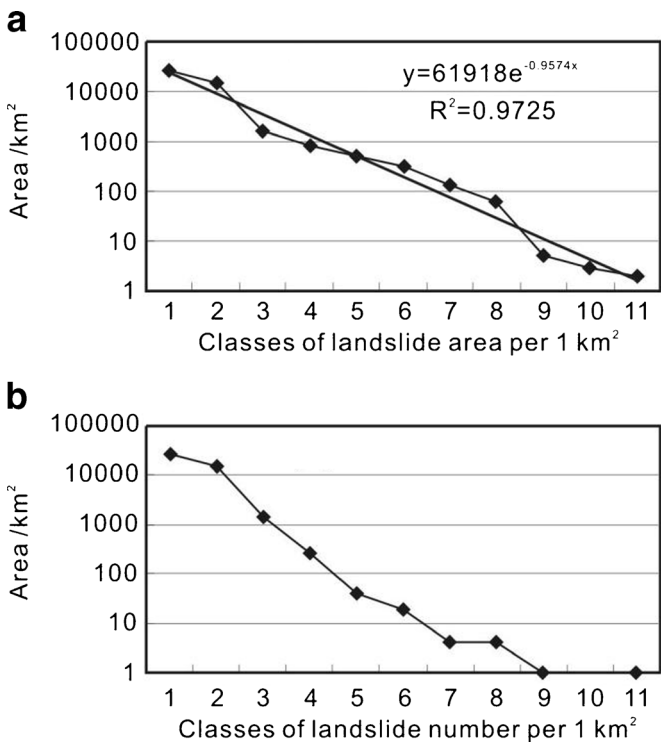

Fig. 5 Correlation curves of LAP, LND with area distribution. **a** LAP; **b** LND (centroid)

are presented in Fig. 7a. Correlations between this classification and the LAP, LND-centroid, and LND-top values are also displayed in Fig. 7a. As the slope curvature values move further away from zero, the susceptibility to landsliding is observed to increase. Rugged slope (both concave and convex slopes) failures occur during strong ground shocking. This interesting phenomenon has received little attention in earthquake-triggered landslide spatial distribution statistical analysis. Another phenomenon is of interest, which involves the higher LND-centroid values compared with the LND-top values for concave slopes (classes 1–6). In turn, for convex slopes, the LND-top values are higher than the LND-centroid values (classes 9–12). In our opinion, the top point of a landslide tends to be on a mountain peak, which represents a convex slope. Therefore, the curve of LND-top values tends to have positive curvatures. Figure 7b presents another classification for slope curvature. Absolute values of the curvature were used in

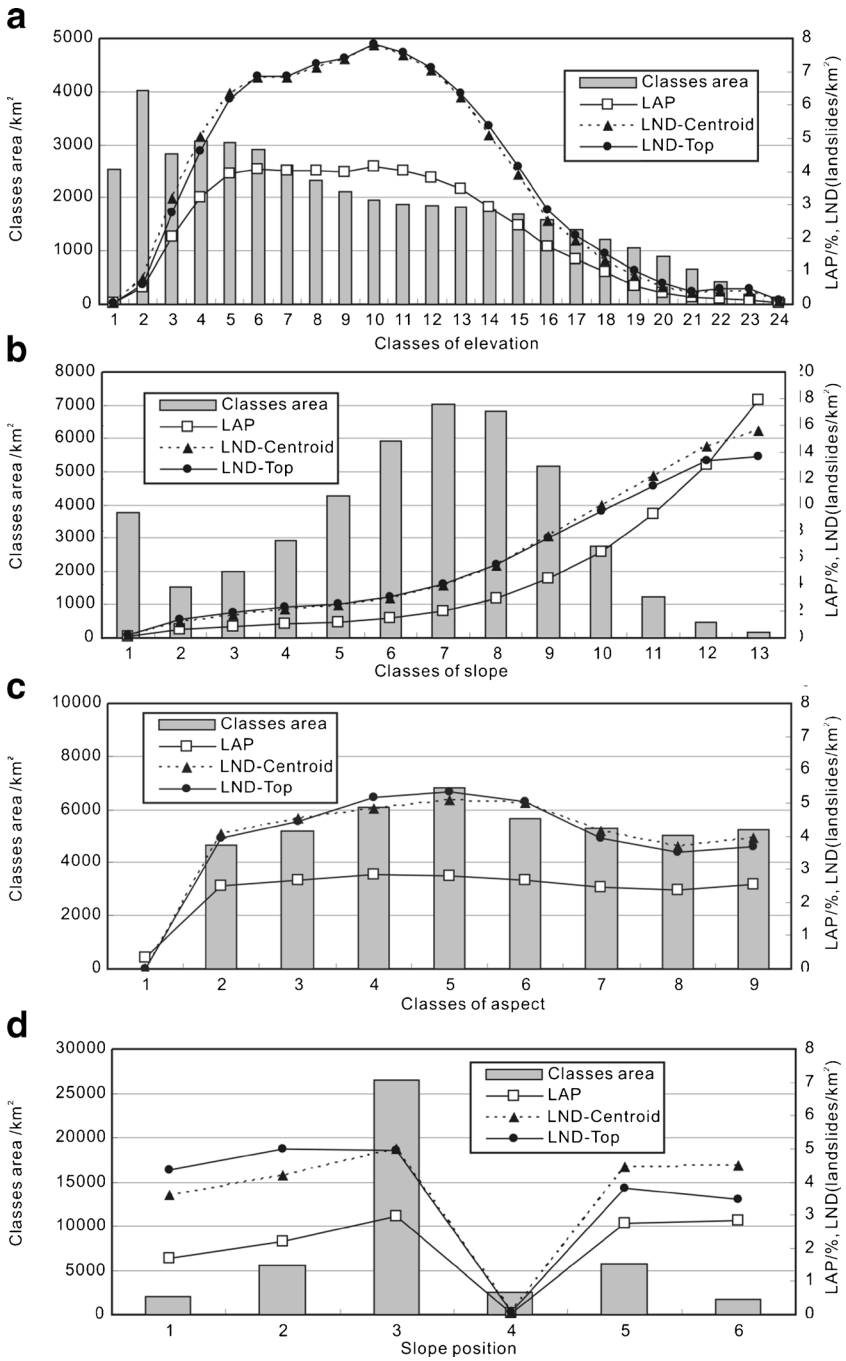

Fig. 6 Relationships between landslide occurrence and topographic parameters. **a** Elevation: *1* <600 m, *2* 600–800 m, *3* 800–1,000 m, *4* 1,000–1,200 m, *5* 1,200–1,400 m, *6* 1,400–1,600 m, *7* 1,600–1,800 m, *8* 1,800–2,000 m, *9* 2,000–2,200 m, *10* 2,200–2,400 m, *11* 2,400–2,600 m, *12* 2,600–2,800 m, *13* 2,800–3,000 m, *14* 3,000–3,200 m, *15* 3,200–3,400 m, *16* 3,400–3,600 m, *17* 3,600–3,800 m, *18* 3,800–4,000 m, *19* 4,000–4,200 m, *20* 4,200–4,400 m, *21* 4,400–4,600 m, *22* 4,600–4,800 m, *23* 4,800–5,000 m, and *24* >5,000 m. **b** Slope angle: *1* 0–5°, *2* 5–10°, *3* 10–15°, *4* 15–20°, *5* 20–25°, *6* 25–30°, *7* 30–35°, *8* 35–40°, *9* 40–45°, *10* 45–50°, *11* 50–55°, *12* 55–60°, and *13* >60°. **c** Slope aspect: *1* flat, *2* N, *3* NE, *4* E, *5* SE, *6* S, *7* SW, *8* W, and *9* NW. **d** Slope position: *1* ridge, *2* upper slope, *3* middle slope, *4* flat slope, *5* lower slope, and *6* valley

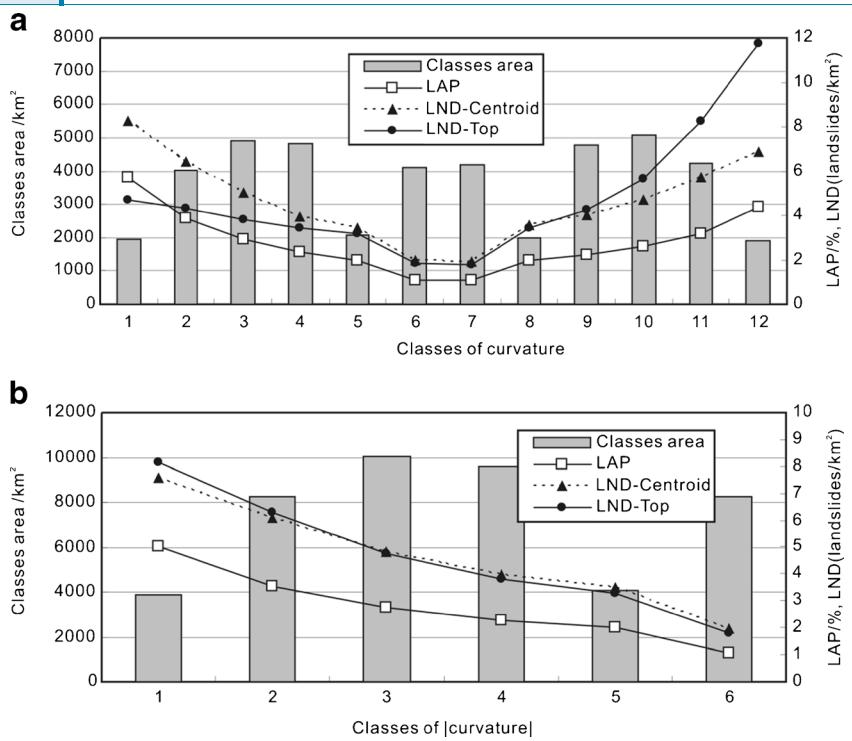

Fig. 7 Relationships between landslide occurrence and slope curvature. **a** Consider the sign of slope curvature: *1* <−2, *2*−2 to−1, *3*−1 to−0.5, *4*−0.5 to −0.2, *5*−0.2 to−0.1, *6*−0.1 −0, *7* 0 −0.1, *8* 0.1 −0.2, *9* 0.2 −0.5, *10* 0.5 −1, *11* 1 −2, and *12* >2. **b** Ignore the sign of slope curvature: *1* <−2 and >2, *2*−2 to−1 and 1 −2, *3*−1 to−0.5 and 0.5 −1, *4*−0.5 to−0.2 and 0.2 −0.5, *5*−0.2 to−0.1 and 0.1 −0.2, and *6*−0.1 −0.1

Fig. 7b, which reveals that landslide occurrence is more difficult as flat slopes are approached. In addition, area distributions of the six slope curvature classifications are also presented in Fig. 7b.

Correlation with lithology

To investigate the relationship between lithology and landslides, a geological map on a scale of 1:200,000 from China Geological Survey was used to provide information on lithology of the study area. Lithology is widely recognized to play an important role in determining landslide hazard because different geological units have different susceptibilities to landslide occurrence, even when the slope failure is not triggered by an earthquake. Lithological and structural variations often lead to a difference in the strength and permeability of rocks and soils. In the study area, the lithology was divided into 20 categories (as indicated in Table 3). Area distributions of the 20 lithology classifications are presented in Fig. 8. The lithology map in vector format was converted into raster format at 20 m × 20 m resolution using GIS software. As demonstrated by the LAP and LND values in Fig. 8, sandstone and siltstone (Z) (class 17) have the most concentrated landslide activity with 12.490 % for the LAP and LND values of 19.147 and 18.996 landslides/km², respectively. The class 20 of granitic rocks has slightly lower LAP and LND values, 12.385 %, and 18.675 and 18.681 landslides/km², respectively. Furthermore, sandstone, siltstone, chert, and slate (Є) (class 16) follows, with one LAP and two LND values, 11.143 %, and 12.151 and 12.186 landslides/km², respectively. In addition, although limestone (T), and schist and andesite (PZ) (classes 4 and 19) exhibit lower LAP values (5.972 and 8.616 %), higher LND values (12.647 and 12.841 landslides/km², respectively, for class 4 and 13.092 and 13.176 landslides/km², respectively, for class 19) can be observed.

Correlations with seismic parameters

The correlations between landslide occurrences and earthquakes were investigated using five different seismic parameters: (1) distance from coseismic fault ruptures (Xu et al. 2008b, 2009b, 2009c), (2) distance from the epicenter, (3) PGA, (4) seismic intensity, and (5) coseismic horizontal surface displacement, coseismic vertical surface displacement, and coseismic total surface displacement (De Michele et al. 2010; Wang et al. 2011; Shen et al. 2009). According to the empirical relationships between maximum epicentral distance, maximum distance to fault plane projection, and Richter earthquake magnitude (Keefer 1984; Rodriguez et al. 1999), a Ms 8.0 earthquake corresponds to approximately 400 km for the upper limits of both the maximum epicentral distance and maximum distance to the fault plane projection. Therefore, the maximum epicentral distance (approximately 400 km) related to the 2008 Ms 8.0 Wenchuan earthquake is equal to the upper value from the statistical result using other earthquake cases from Keefer (1984) and Rodriguez et al. (1999). The maximum distance to the fault plane projection (approximately 200 km) related to the 2008 Ms 8.0 Wenchuan earthquake is less than the upper value from the statistical result using other earthquake cases from Keefer (1984) and Rodriguez et al. (1999).

In general, there was a good correlation between the distance from the main surface ruptures and the spatial distribution patterns of earthquake-triggered landslide. The Yingxiu-Beichuan fault rupture, the major surface rupture, was used to construct

Table 3 Geologic unit and descriptions in the study area

No.	Geologic unit	Description of lithology	Area (km^2)	Ls area (km^2)	LAP (%)
1	Q	Unconsolidated deposits	3,494.455	7.132	0.204
2	K~N	Conglomerate, sandstone, siltstone, shale, and mudstone	1,222.606	0.513	0.042
3	J	Sandstone and siltstone interbedded with shale, claystone and siltstone intercalated with sandstone, conglomerate	1,810.815	4.501	0.249
4	T	Limestone	299.518	17.888	5.972
5	T	Sandstone, siltstone interbedded with phyllite, shale, mudstone, phyllite, and siltstone	10,102.104	80.295	0.795
6	P	Limestone and shale	333.997	18.820	5.635
7	P	Limestone	698.298	37.589	5.383
8	C-P	Limestone, phyllite, and basalt	1,145.921	12.835	1.120
9	C	Limestone	215.597	11.366	5.272
10	C	Limestone, slate, phyllite, and sandstone	22.724	0.003	0.014
11	D	Limestone and sandstone	1,158.133	45.469	3.926
12	D	Phyllite and limestone	3,873.044	57.398	1.482
13	S	Phyllite, slate, sandstone, siltstone, and limestone	1,083.450	14.948	1.380
14	S	Phyllite, schist, slate, sandstone, and limestone	6,902.662	119.284	1.728
15	O	Limestone, marl, and slate	332.812	5.347	1.607
16	Є	Sandstone, siltstone, chert, and slate	856.737	95.470	11.143
17	Z	Sandstone and siltstone	583.237	72.848	12.490
18	PZ	Quartz sandstone, feldspathic sandstone, phyllite, slate, and metamorphic sandstone	5,366.958	11.626	0.217
19	PZ	Schist and andesite	623.947	53.757	8.616
20		Granitic rocks	3,904.1152	483.5336	12.385

the correlation between landslide occurrences and the major surface. For the distance from the surface fault rupture, compared with the buffer distance of epicenter, a lower buffer distance of 2 km was selected to construct the buffer map (Fig. 9a). There are 48 classes of distance from the Yingxiu-Beichuan fault on a hanging wall and 22 classes on a footwall. Area distributions for classifications of distance from the main surface fault rupture are indicated in Fig. 10a and b, respectively. In addition, Fig. 10a illustrates the variations of the LAP and LND values with distance from the Yingxiu-Beichuan fault. As demonstrated in Fig. 10a, the highest LAP and LND values are adjacent to the fault, with values decreasing rapidly as the distance is increased. The LAP and the two types of LND values are as high as 10.261 %, and 17.645 and 17.579 landslides/km^2, respectively, within 2 km of the Yingxiu-

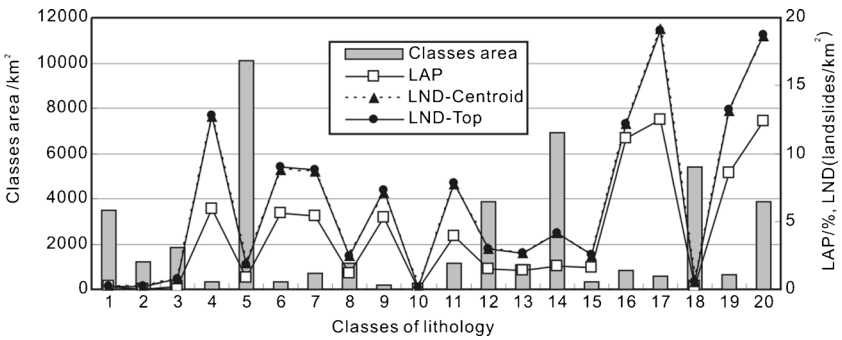

Fig. 8 Relationships between landslide occurrence and lithology. *1* Unconsolidated deposits (Q), *2* conglomerate, sandstone, siltstone, shale, and mudstone (K~N), *3* sandstone and siltstone interbedded with shale, claystone, and siltstone intercalated with sandstone, conglomerate (J), *4* limestone (T), *5* sandstone, siltstone interbedded with phyllite, shale, mudstone, phyllite, and siltstone (T), *6* limestone and shale (P), *7* limestone (P), *8* limestone, phyllite, and basalt (C-P), *9* limestone (C), *10* limestone, slate, phyllite, and sandstone (C), *11* limestone and sandstone (D), *12* phyllite and limestone (D), *13* phyllite, slate, sandstone, siltstone, and limestone (S), *14* phyllite, schist, slate, sandstone, and limestone (S), *15* limestone, marl, and slate (O), *16* sandstone, siltstone, chert, and slate (Є), *17* sandstone and siltstone (Z), *18* quartz sandstone, feldspathic sandstone, phyllite, slate, and metamorphic sandstone (PZ), *19* schist and andesite (PZ), *20* granitic rocks

Beichuan surface fault rupture. Landslides at distances greater than 30 km were rare.

In addition, to compare the differences of the LAN and LND values for the hanging wall and the footwall, the LAP and LND values were calculated for both sides of the Yingxiu-Beichuan surface fault rupture (Fig. 10b). Most of the landslides (146,708 landslides, 74.86 % of the total landslide number, and these landslides composed an area of 924.089 km^2, 80.31 % of the total landslide area) occurred on the hanging wall. Similar to our previous statistical results (Dai et al. 2011), the landslides were concentrated on the hanging wall of the Yingxiu-Beichuan surface fault rupture. The highest LAP and LND values occurred along the rupture on both the hanging wall and the footwall. The LAP and LND values were as high as 13.391 %, and 22.117 and 22.117 landslides/km^2, respectively, within 2 km of the fault rupture on the hanging wall. On the footwall, within 2 km of the fault rupture, these values were 7.106 %, and 13.136 and 13.005 landslides/km^2, respectively. Furthermore, the LAP and the two LND values decreased rapidly as the distances increased for both the hanging wall and the footwall. In summary, the LAP and two LND values exhibit strong correlations with distance from the Yingxiu-Beichuan surface fault ruptures.

As indicated in a previous paper (Dai et al. 2011), the correlation between landslide occurrence and distance from the epicenter is complicated; nevertheless, there is a lack of landslide data near the epicenter. In this paper, the LAP and LND values were determined for a sequence of 5-km-wide concentric bands extending outward from the source (Fig. 9b). The outer bands were truncated where they intersected the study area boundary. There are 60 classes of distance from the epicenter. Figure 11a illustrates the

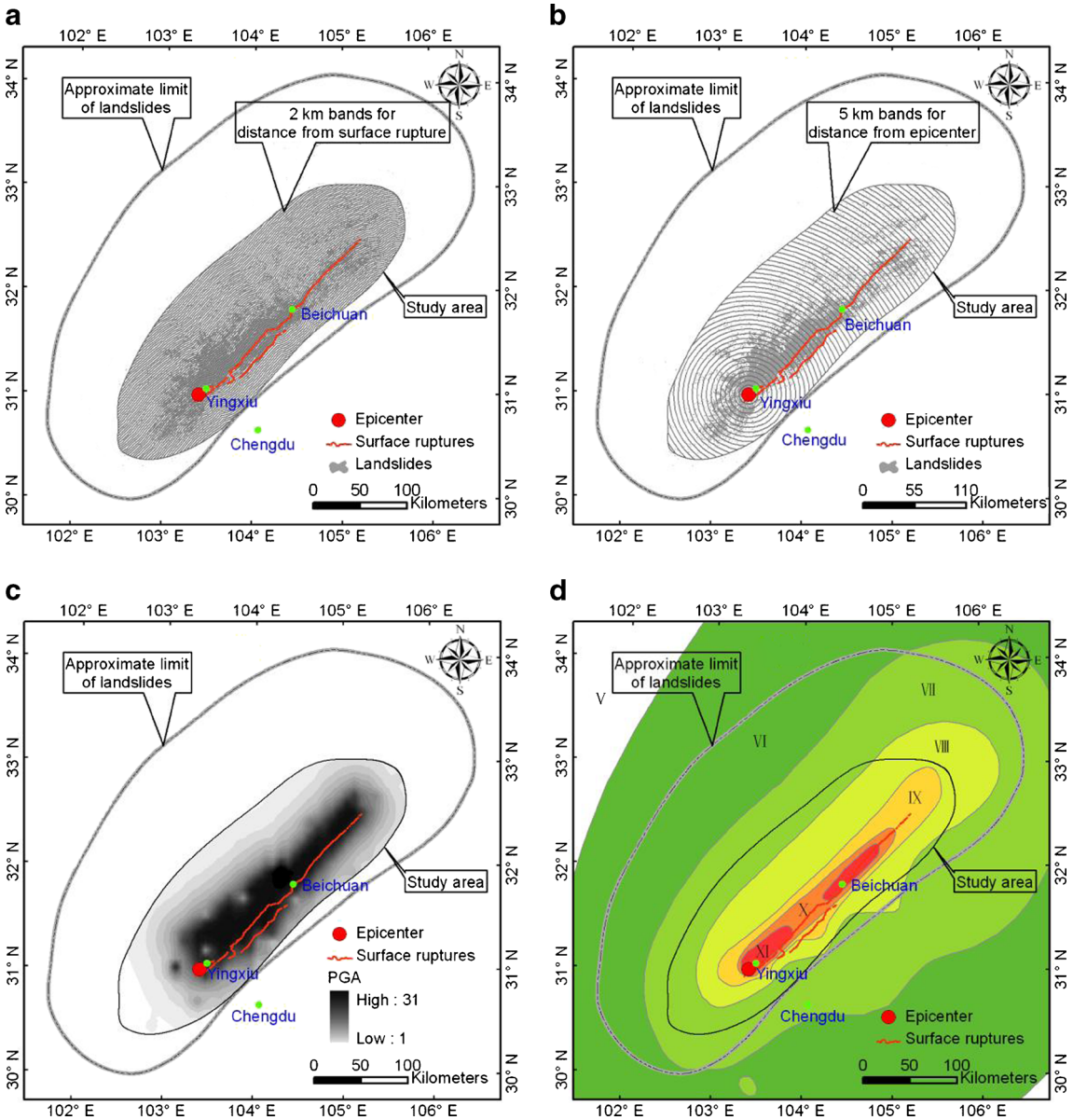

Fig. 9 Distribution maps of seismic parameters of the 2008 Wenchuan earthquake. **a** 2-km bands for classifying distance from the Yingxiu-Beichuan surface fault rupture; **b** 5-km bands for classifying distance from epicenter; **c** distribution map of PGA; **d** seismic intensity map

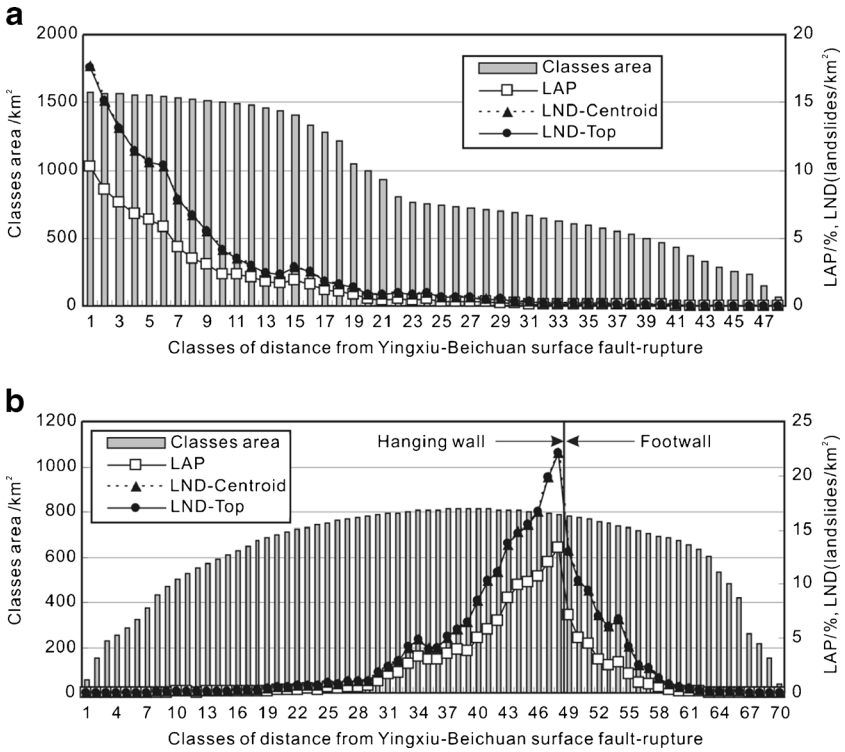

Fig. 10 Relationships between landslide occurrence and distance from the Yingxiu-Beichuan surface fault rupture. **a** Statistics with hanging wall and footwall; **b** respective hanging wall and footwall, 2-km intervals, 48 classes on the hanging wall, and 22 classes on the footwall

variations in the LAP and two LND values with distance from the epicenter and presents the area distributions of the 60 classifications. The highest LAP and LND values are observed near the epicenter. The LAP and two LND values are as high as 17.982 %, and 60.148 and 59.995 landslides/km^2, respectively, within 5 km of the epicenter. Furthermore, both the LAP and LND values decrease rapidly as the distances increase.

In general, there was a good correlation between the distribution of earthquake-triggered landslides and ground shaking. The US Geological Survey (2008) created a PGA map based on the peak ground motion amplitudes recorded on seismic sensors (accelerometers), with interpolation based on both estimated amplitudes where data are lacking, and site amplification corrections (Dai et al. 2011). Most of the study area experienced high levels of ground shaking during the Wenchuan earthquake. A regional contour map of PGA from USGS (2008) indicated PGA values from 0.12 to 1.30 g in the study area (Fig. 9c). There are 31 classes of PGA values (as shown in Fig. 11). Figure 11b illustrates the correlations of the LAP and two LND values with PGA. In addition, the area distribution of the 31 PGA classes is also presented in Fig. 11b. Surprisingly, there is no clear trend between the LAP and two LND values, and the PGA values. The area distribution of the PGA classes resulted in a seemingly irregular pattern between landslide occurrence and the PGA values. In fact, the PGA values exceeding 0.88 g (classes of 20–31) only cover 383.026 km^2, or approximately 0.87 % of the total study area. The area is too small to obtain objective statistical results. For PGA values of 0.12–0.84 g (classes 1–19), increasing PGA values show a positive correlation with increasing LAP and LND values. The LAP and two LND values are as high as 15.635 %, and 21.09 and 21.11 landslides/km^2, respectively, within the area of PGA values equal to 0.84 g (Fig. 11b). The LAP and LND values increase rapidly with an increase in the PGA values within the range of 0.12–0.84 g. Abnormal slightly higher LAP and LND values are observed at 0.68 g (class 15) for the PGA. We can conclude that the LAP and LND values increase with increasing PGA values.

The seismic intensity map was produced by the China Earthquake Administration (CEA) (Fig. 9d), and the classes of seismic intensity in the study area include VII, VIII, IX, X, and XI. Figure 11c presents the variations of the LAP and LND values with the seismic intensity and the area distributions of the VII, VIII, IX, X, and XI intensity zones. As expected, both the LAP and two LND values increase as the seismic intensity grades increase, with the highest values occurring where the seismic intensity is XI. The LAP and two LND values are as high as 17.852 %, and 28.487 and 28.489 landslides/km^2, respectively, within the XI intensity district (Fig. 11c).

Synthetic aperture radar (SAR) technology provides us with a good opportunity to determine the correlation between landslide occurrence and coseismic surface displacement. De Michele et al. (2010) combined C- and L-band SAR offset data from ascending and descending tracks to invert the 3-D surface displacement in the near coseismic field of the Wenchuan earthquake. Their data, coupled with a simple elastic dislocation model, provide new results that strongly suggest the presence of a blind thrust striking along the range front and being active at depths during the earthquake. Furthermore, Wang et al. (2011) produced 38 stations of continuous GPS data, 435 sites of campaign GPS data, and 33 sites of triangulation sites, resurveyed with GPS after the earthquake. In addition, Shen et al. (2009) produced 158 GPS data. These ground-based measurements of surface displacement for the 2008 Wenchuan earthquake were used to supplement the results from De Michele et al. (2010). The area beyond the study area from De Michele et al. (2010)

is interpolated using the GPS data from Wang et al. (2011) and Shen et al. (2009). Then, three surface displacement (horizontal, vertical, and total) grid layers with 20 m×20 m resolution were constructed in the ArcGIS platform. The classes of each layer are listed in Fig. 13. The classification maps of surface displacement are presented in Fig. 12a, b, and c. Figure 13a, b, and c show the LAP and two LND values for the three surface displacement (horizontal, vertical, and total) values and the area distribution of the classes of the three surface displacement layers. Both of these figures reveal a general correlation that the LAP and two LND values increase with increasing coseismic surface displacement. However, several abnormal LAP and LND values are observed in the classes where the surface displacements exceed 3 m (classes after 12). We consider the main reason for these abnormalities to be the small area covered by these classes. For the other cases, it appears that surface displacement exceeding 3 m is sufficient to trigger landslides, and other factors may control landslide distribution in areas suffering high surface displacement.

Comparison of the effect of eight impact factors on landslides

A bivariate statistical method was selected to compare the effect of eight impact factors on landslide occurrence. Eight impact factors including slope angle, slope curvature, lithology, distance from the epicenter, distance from the Yingxiu-Beichuan surface fault rupture, PGA, seismic intensity, and coseismic surface displacement were selected as the objects for comparison. We assume that the eight factors are conditionally independent of one another for earthquake-triggered landslides. Descending (landslide occurrence) cumulative curves of the cumulative percentage area of ranks and the percentage of landslide occurrence (measured by one LAP and two LNDs) were constructed. As described above, there were continuous positive or negative correlations between earthquake-triggered landslide occurrence and controlling factors, including slope angle, slope curvature, distance from the epicenter, distance from the Yingxiu-Beichuan surface fault rupture, PGA, seismic intensity, and coseismic surface displacement. Therefore, the cumulative curves of these factors are constructed from ranks

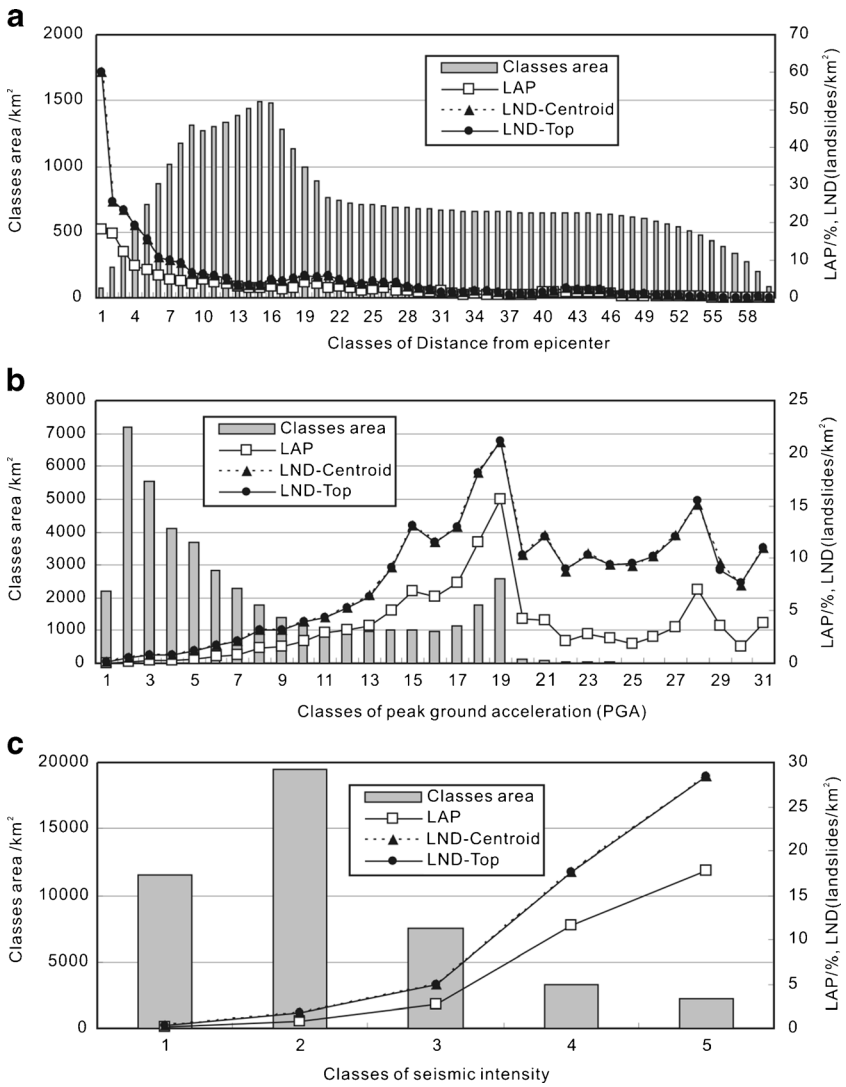

Fig. 11 Relationships between landslide occurrence and seismic parameters. **a** Distance from epicenter, 5-km intervals, 60 classes; **b** PGA: *1* 0.12 g, *2* 0.16 g, *3* 0.20 g, *4* 0.24 g, *5* 0.28 g, *6* 0.32 g, *7* 0.36 g, *8* 0.40 g, *9* 0.44 g, *10* 0.48 g, *11* 0.52 g, *12* 0.56 g, *13* 0.60 g, *14* 0.64 g, *15* 0.68 g, *16* 0.72 g, *17* 0.76 g, *18* 0.80 g, *19* 0.84 g, *20* 0.88 g, *21* 0.92 g, *22* 0.96 g, *23* 1.00 g, *24* 1.04 g, *25* 1.08 g, *26* 1.12 g, *27* 1.16 g, *28* 1.20 g, *29* 1.24 g, *30* 1.28 g, *31* 1.30 g. **c** Seismic intensity: *1* VII, *2* VIII, *3* IX, *4* X, *5* XI

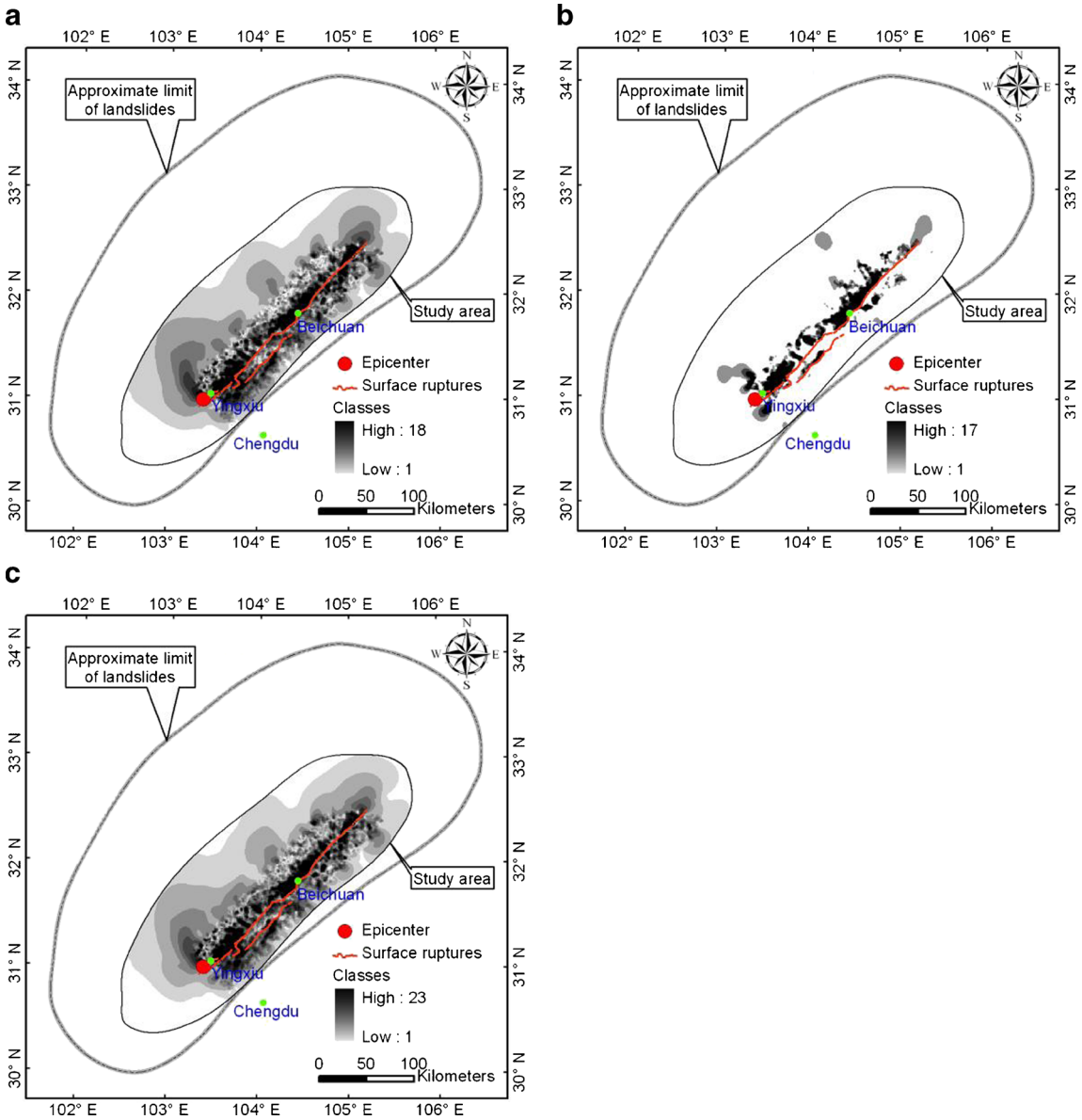

Fig. 12 Coseismic surface displacement maps. **a** Horizontal displacement; **b** vertical displacement; **c** total displacement

of the highest effect on landslide occurrence for the eight factors. These ranks are the steepest slope angle rank (>60°, class 60), the most rugged slopes base on curvature (<−2 and >2, class 1), the nearest distance from the epicenter (<5 km, class 1), the nearest distance from the Yingxiu-Beichuan surface fault rupture rank (<2 km, class 1), the highest PGA value (1.30 g, class 31), the maximum seismic intensity (XI, class 5), and the largest coseismic total surface displacement (>5.5 m, class 23). For the lithology, a discrete factor, orders of the 20 classes effect on landslide occurrence, was based on the LAP and two LND values. The cumulative percentage area curves for lithology are constructed by ordering from 1 to 20 the LAP and two types of LND (as shown in Fig. 14). The area under the cumulative curve (AUC) is used as the contrast factor to compare the effects on landslide occurrence.

The comparison of the LAP and two LND AUC values, as shown in Table 4, of the eight impact factors revealed that PGA and seismic intensity have the most significant effects on earthquake-triggered landslides. The LAP and AUC values' descending order of the eight impact factors are PGA > seismic intensity > lithology > distance from the Yingxiu-Beichuan surface fault rupture > surface displacement > slope angle > distance from the epicenter > slope curvature. The two groups of LND AUC values' descending order of the eight impact factors are seismic intensity > PGA > distance from the Yingxiu-Beichuan surface fault rupture > lithology > surface displacement > distance from the epicenter > slope angle > slope curvature. The AUC values of the LAP and two types of LND revealed a generally similar order for the eight landslide controlling parameters. Seismic parameters including the PGA and seismic intensity had the most significant effect on landslide occurrence, followed by the geologic parameter (lithology). The topographical parameters, such as slope angle and slope curvature, had minimal effect on the landslide concentration.

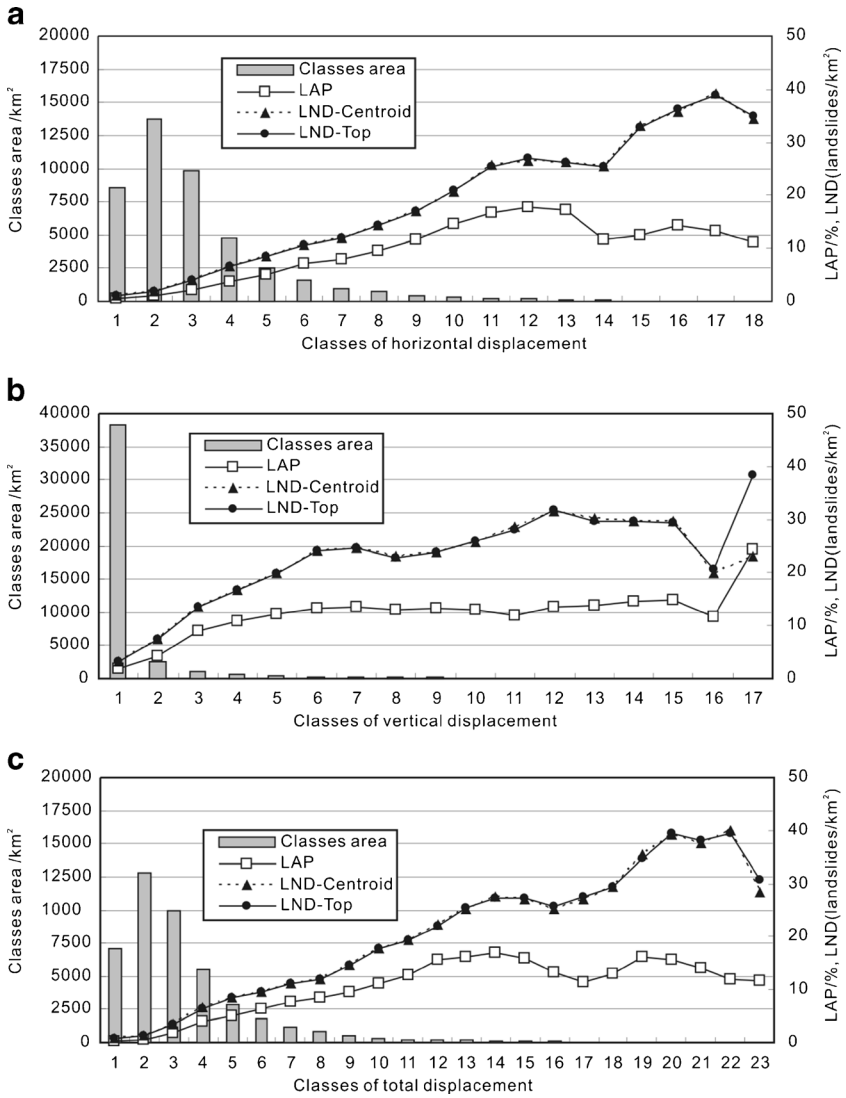

Fig. 13 Relationships between landslide occurrence and surface displacement. **a** Coseismic horizontal surface displacement: *1* 0 –0.25 m, *2* 0.25 –0.5 m, *3* 0.5 –0.75 m, *4* 0.75 –1 m, *5* 1.0 –1.25 m, *6* 1.25 –1.5 m, *7* 1.5 –1.75 m, *8* 1.75 –2.0 m, *9* 2.0 –2.25 m, *10* 2.25 –2.5 m, *11* 2.5 –2.75 m, *12* 2.75 –3.0 m, *13* 3.0 –3.25 m, *14* 3.25 –3.5 m, *15* 3.5 –3.75 m, *16* 3.75 –4.0 m, *17* 4.0 –4.25 m, *18* >4.25 m. **b** Coseismic vertical surface displacement: *1* 0 –0.25 m, *2* 0.25 –0.5 m, *3* 0.5 –0.75 m, *4* 0.75 –1 m, *5* 1.0 –1.25 m, *6* 1.25 –1.5 m, *7* 1.5 –1.75 m, *8* 1.75 –2.0 m, *9* 2.0 –2.25 m, *10* 2.25 –2.5 m, *11* 2.5 –2.75 m, *12* 2.75 –3.0 m, *13* 3.0 –3.25 m, *14* 3.25 –3.5 m, *15* 3.5 –3.75 m, *16* 3.75 –4.0 m, *17* >4.0 m. **c** Coseismic total surface displacement: *1* 0 –0.25 m, *2* 0.25 –0.5 m, *3* 0.5 –0.75 m, *4* 0.75 –1 m, *5* 1.0 –1.25 m, *6* 1.25 –1.5 m, *7* 1.5 –1.75 m, *8* 1.75 –2.0 m, *9* 2.0 –2.25 m, *10* 2.25 –2.5 m, *11* 2.5 –2.75 m, *12* 2.75 –3.0 m, *13* 3.0 –3.25 m, *14* 3.25 –3.5 m, *15* 3.5 –3.75 m, *16* 3.75 –4.0 m, *17* 4.0 –4.25 m, *18* 4.25 –4.5 m, *19* 4.5 –4.75 m, *20* 4.75 –5.0 m, *21* 5.0 –5.25 m, *22* 5.25 –5.5 m, *23* >5.5 m

Analysis and discussions

As stated by Keefer (2002) and Harp et al. (2011a), a highly accurate and complete landslide inventory is an essential component of seismic landslide hazard analysis. In the following text, some qualitative comparisons between our results and previously published results were made. In this paper, 196,007 landslides, with an area of 1,150.622 km^2, were used to perform seismic landslide spatial analysis, which can be compared with the 56,000 landslides, with a total area of approximately 811 km^2, studied by Dai et al. (2011); the nearly 60,000 landslides studied by Gorum et al. (2011); and the 11,306 landslides studied by Huang and Li (2009). The number and area of the new (nearly) complete landslide inventory is approximately 350 and 142 % of the results from Dai et al. (2011), approximately 327 % of the results from Gorum et al. (2011), and approximately 1,734 % of the results from Huang and Li (2009) based on the number of landslides. Therefore, there is a large difference between the new inventories and these previously published papers, especially the point inventories. Huang and Li (2009) produced the landslide inventory only for emergency investigation. The inventory of landslides triggered by the Wenchuan earthquake from Dai et al. (2011) did not cover the entire earthquake-triggered landslide affected area because some areas lacked (high-resolution) remote sensing images. Therefore, in our opinion, these landslide inventories are incomplete.

The LAP and two types of LND values in each class of all the controlling parameters based on the new database were much higher than the previous results (e.g., Dai et al. 2011; Gorum et al. 2011). A detailed comparison of the relative relationship among different

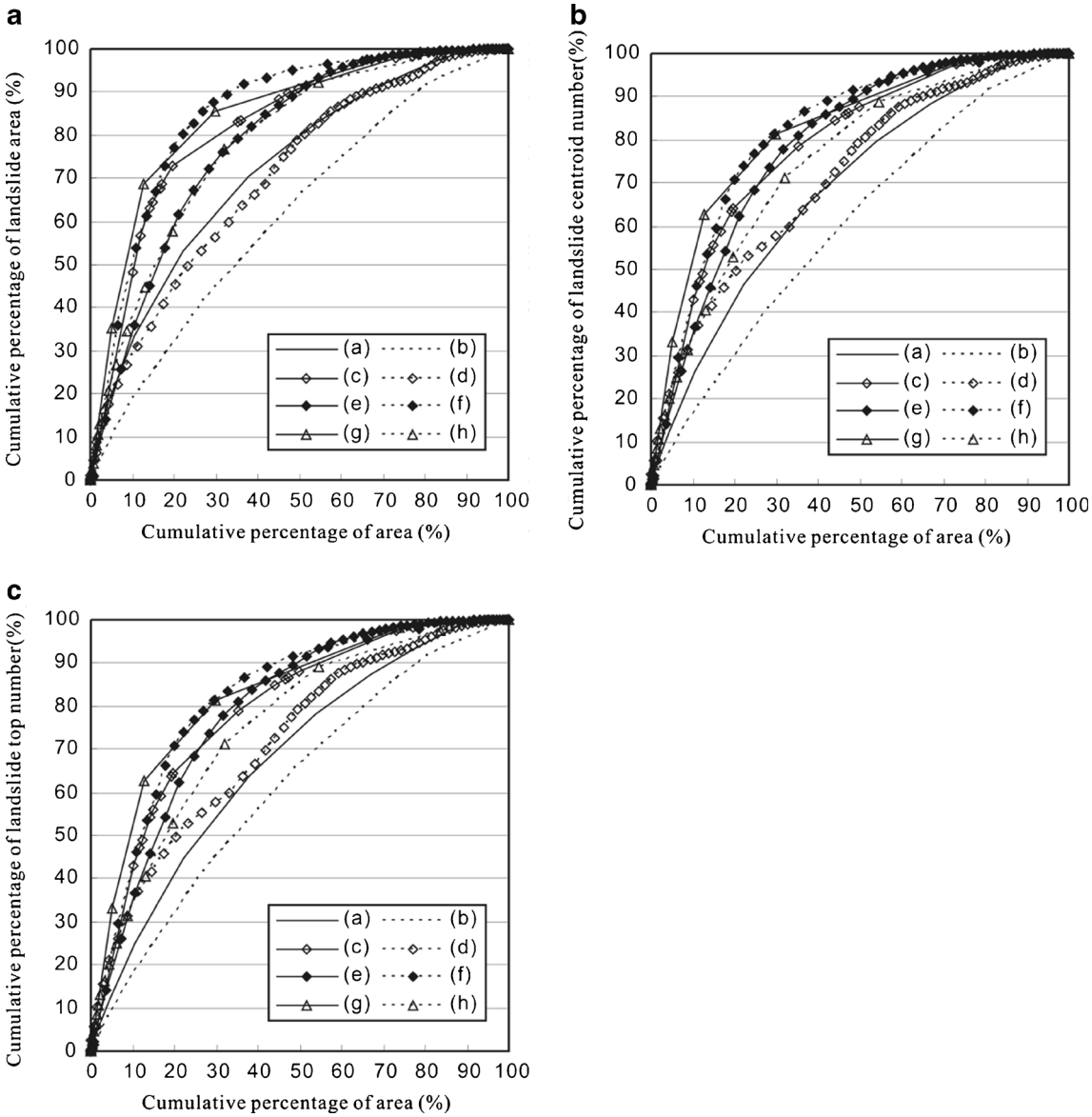

Fig. 14 Comparison of influence on landslide occurrence for five impact factors. **a** Landslide area; **b** landslide centroid point number; **c** landslide top point number. *a* slope angle, *b* slope curvature, *c* lithology, *d* distance from epicenter, *e* distance from the Yingxiu-Beichuan surface fault rupture, *f* PGA, *g* seismic intensity, *h* coseismic surface displacement

Table 4 Comparing of AUC values of landslide area and landslide number

Impact factors	AUC for area order)	AUC for number centroid (order)	AUC for number top (order)
(A) Slope angle	72.391 (6)	68.867 (7)	67.764 (7)
(B) Slope curvature	61.325 (8)	60.257 (8)	61.495 (8)
(C) Lithology	81.919 (3)	78.865 (4)	78.961 (4)
(D) Distance from epicenter	70.400 (7)	71.748 (6)	71.742 (6)
(E) Distance from surface rupture	78.695 (4)	79.081 (3)	79.070 (3)
(F): PGA	84.887 (1)	81.528 (2)	81.529 (2)
(G): Seismic intensity	84.722 (2)	82.341 (1)	82.336 (1)
(H): Surface displacement	78.148 (5)	75.158 (5)	75.177 (5)

classes of each controlling parameter was also performed. For the relation between elevation and landslide occurrence, in this paper, the most concentrated landslide areas were located between 1,200- and 3,000-m elevation relatively compared with the 750 - to 1,500-m elevation range cited in our original landslide inventory (Dai et al. 2011). In our opinion, this result occurred because there was no landslide data in some areas around the epicenter. These areas are mainly located at elevations between 1,000 and 3,000 m. In addition, the distance from the epicenter is another obvious difference. Our published paper (Dai et al. 2011) revealed a complex correlation between landslide occurrence and the distance from the epicenter of the earthquake, rather than a simple negative correlation, as observed in other reported cases of earthquakes. In contrast, our new results exhibit a good correlation between landslide occurrence and distance from the epicenter, and both the LAP and two LND values decrease rapidly as this distance increases. The statistical results of lithology also show a significant difference; sandstone, siltstone (Z), and granitic rocks exhibit the maximum LAP and LND values from this study; carbonate and igneous rocks exhibit the most landslide concentration according to Gorum et al. (2011); and schist (PZ), sandstone, and siltstone intercalated with slate (Є) exhibit the largest LAP and LND values according to our published paper (Dai et al. 2011). In addition to these results, the statistical results concerning other factors (e.g., slope angle, slope aspect, and distance from the Yingxiu-Beichuan surface fault rupture) demonstrate tendencies similar to those reported in other publications (Dai et al. 2011; Gorum et al. 2011). The comparisons indicate that some of the results obtained from analyzing incomplete landslide distribution data are not objective. Therefore, it is necessary and important to produce a complete and detailed landslide inventory for subsequent seismic landslide studies.

Furthermore, Harp et al. (2011a) also considered the images should ideally meet the following criteria: they (1) must be continuous and span the entire landslide distribution, (2) must have a resolution that allows identification of individual landslides as small as a few meters across, (3) must have stereo coverage or be able to be draped over a digital elevation model to obtain a stereolike perspective view, and (4) must be as cloud-free as possible and be acquired as soon as possible after the earthquake to capture the initial aspects of the landslides and the terrain or infrastructure that they affect. Although a huge number of 197,481 landslide polygons are present in our new inventory, it is more appropriate considering that it is a nearly complete landslide inventory rather than a strictly complete inventory because large areas are affected by the earthquake and a large number of landslides occurred. It is very difficult to obtain a rigorously complete landslide inventory following the landslide inventory criteria and mapping criteria (Harp et al. 2011a) for several reasons such as: commercially based satellite imagery with resolutions of less than 1 m is often expensive, the rapid access to high resolution satellite imagery in a large area several days after the earthquake is rather difficult, and the weather is often cloudy in the Wenchuan earthquake struck area. Therefore, strictly speaking, we have failed to obtain complete coverage of landslide distributions triggered by the 2008 Wenchuan earthquake. In our opinion, the three landslide inventories are nearly complete and sufficient to perform objective seismic landslide spatial distribution and hazard analyses, as stated in Harp et al. (2011a).

Conclusions

In conclusion, we mapped 197,481 landslide polygons from visual interpretation of aerial photographs and satellite images and by selected field verification. Three nearly complete inventories were constructed, including landslide polygons, landslide centroid points, and landslide top points. Density maps of the landslide areas and numbers (centroid) were constructed. Most of the landslides were observed to be concentrated along the Yingxiu-Beichuan surface fault rupture, and most of the landslides occurred on the hanging wall. Landslide occurrence exhibits a continuous correlation (positive or negative) with slope angle, slope curvature, distance from the epicenter and the Yingxiu-Beichuan surface fault rupture, PGA, seismic intensity, and coseismic surface displacement. The highest LAP and LND values occurred at elevations ranging from 1,200 to 3,000 m. The landslides have preferred orientations, dominated by the eastern, southeastern, and southern directions. The sandstone, siltstone (Z), and granitic rocks experience more concentrated earthquake-triggered landslides. No obvious correlations were observed between LAP and the two LND values, and the slope position. The results of the bivariate statistical method for comparison of the effect of several factors on landslide occurrence revealed the following descending order of the 2008 Wenchuan earthquake-triggered landslide impact factors: PGA > seismic intensity > lithology > distance from the Yingxiu-Beichuan surface fault rupture > surface displacement > slope angle > distance from the epicenter > slope curvature according to the LAP values. According to the LND values, we observed that the effect of the impact factors descended in the following order: seismic intensity > PGA > distance from the Yingxiu-Beichuan surface fault rupture > lithology > surface displacement > distance from the epicenter > slope angle > slope curvature.

Acknowledgments

This research is supported by the National Science Foundation of China (grant no. 41202235). We thank Dr. Cees J. van Westen, Dr. Tolga Gorum, Dr. Suning Xu, Dr. Feng Shi, Dr. Honglin He, and Master Xiyan Wu for their help in providing some remote sensing images for compiling the inventory of landslides. We also thank Marcello de Michele for his assistance in providing surface displacement data. We appreciate Dr. Cees J. van Westen, the editor, and anonymous reviewers for their great assistances in paper writing and useful suggestions that improved the manuscript.

References

Alfaro P, Delgado J, García-Tortosa FJ, Lenti L, López JA, López-Casado C, Martino S (2012) Widespread landslides induced by the Mw 5.1 earthquake of 11 May 2011 in Lorca, SE Spain. Eng Geol 137–138:40–52

Chen JP, Li JF, Qin XW, Dong QJ, Sun Y (2009) RS and GIS-based statistical analysis of secondary geological disasters after the 2008 Wenchuan earthquake. Acta Geol Sin 83(4):776–785

Chigira M, Yagi H (2006) Geological and geomorphological characteristics of landslides triggered by the 2004 Mid Niigta prefecture earthquake in Japan. Eng Geol 82(4):202–221

Chigira M, Wu XY, Inokuchi T, Wang GH (2010) Landslides induced by the 2008 Wenchuan earthquake, Sichuan, China. Geomorphology 118(3–4):225–238

Collins BD, Kayen R, Tanaka Y (2012) Spatial distribution of landslides triggered from the 2007 Niigata Chuetsu–Oki Japan Earthquake. Eng Geol 127:14–26
Dadson SJ, Hovius N, Chen H, Dade WB, Hsieh ML, Willett SD, Hu JC, Horng MJ, Chen MC, Stark CP, Lague D, Lin JC (2003) Links between erosion, runoff variability and seismicity in the Taiwan orogen. Nature 426(6967):648–651
Dadson SJ, Hovius N, Chen H, Dade WB, Lin JC, Hsu ML, Lin CW, Horng MJ, Chen TC, Milliman J, Stark CP (2004) Earthquake-triggered increase in sediment delivery from an active mountain belt. Geology 32(8):733–736
Dadson SJ, Hovius N, Pegg S, Dade WB, Horng MJ, Chen H (2005) Hyperpycnal river flows from an active mountain belt. J Geophys Res 110:F04016
Dai FC, Xu C, Yao X, Xu L, Tu XB, Gong QM (2011) Spatial distribution of landslides triggered by the 2008 Ms 8.0 Wenchuan earthquake, China. J Asian Earth Sci 40(4):883–895
Das JD, Saraf AK, Panda S (2007) Satellite data in a rapid analysis of Kashmir earthquake (October 2005) triggered landslide pattern and river water turbidity in and around the epicentral region. Int J Remote Sens 28(8):1835–1842
De Michele M, Raucoules D, De Sigoyer J, Pubellier M, Chamot-Rooke N (2010) Three-dimensional surface displacement of the 2008 May 12 Sichuan earthquake (China) derived from synthetic aperture radar: evidence for rupture on a blind thrust. Geophys J Int 183(3):1097–1103
Di BF, Zeng HJ, Zhang MH, Ustin SL, Tang Y, Wang ZY, Chen NS, Zhang B (2010) Quantifying the spatial distribution of soil mass wasting processes after the 2008 earthquake in Wenchuan, China: a case study of the Longmenshan area. Remote Sens Environ 114(4):761–771
Fukuoka H, Sassa K, Scarascia-Mugnozza G (1997) Distribution of landslides triggered by the 1995 Hyogo-ken Nanbu earthquake and long runout mechanism of the Takarazuka Golf Course landslide. J Phys Earth 45(2):83–90
Gorum T, Fan XM, van Westen CJ, Huang RQ, Xu Q, Tang C, Wang GH (2011) Distribution pattern of earthquake-induced landslides triggered by the 12 May 2008 Wenchuan earthquake. Geomorphology 133(3–4):152–167
Gorum T, van Westen CJ, Korup O, van der Meijde M, Fan X, van der Meer FD (2013) Complex rupture mechanism and topography control symmetry of mass-wasting pattern, 2010 Haiti earthquake. Geomorphology 184:127–138
Govi M (1977) Photo-interpretation and mapping of the landslides triggered by the Friuli earthquake (1976). Bull Int Assoc Eng Geol 15:67–72
Guzzetti F, Mondini AC, Cardinali M, Fiorucci F, Santangelo M, Chang KT (2012) Landslide inventory maps: new tools for an old problem. Earth Sci Rev 112(1–2):42–66
Han YS, Liu HJ, Cui P, Su FH, Du DS (2009) Hazard assessment on secondary mountain-hazards triggered by the Wenchuan earthquake. J Appl Remote Sens 3(1):031645
Harp EL, Jibson RW (1995) Inventory of landslides triggered by the 1994 Northridge, California earthquake. US Geological Survey. http://pubs.usgs.gov/of/1995/ofr-95-0213/plate1.gif
Harp EL, Jibson RW (1996) Landslides triggered by the 1994 Northridge, California, earthquake. Bull Seismol Soc Am 86(1B):S319–S332
Harp EL, Keefer DK (1990) Landslides triggered by the earthquake. Rymer MJ, Ellsworth WL (eds) the Coalinga, California, Earthquake of May 2, 1983, US Geological Survey Professional Paper 1487: 335–348
Harp EL, Wieczorek GF, Wilson RC (1978) Earthquake-induced landslides from the February 4, 1976 Guatemala earthquake and their implications for landslide hazard reduction. 20 pages. http://cidbimena.desastres.hn/pdf/eng/doc5175/doc5175.htm
Harp EL, Wilson RC, Wieczorek GF (1981) Landslides from the February 4, 1976, Guatemala earthquake. US Geological Survey Professional Paper 1204-A, 35 pages
Harp EL, Tanaka K, Sarmiento J, Keefer DK (1984) Landslides from the May 25–27, 1980, Mammoth Lakes, California, earthquake sequence. US Geological Survey Miscellaneous Investigations Series Map I-1612
Harp EL, Keefer DK, Sato HP, Yagi H (2011a) Landslide inventories: the essential part of seismic landslide hazard analyses. Eng Geol 122(1–2):9–21
Harp EL, Jibson RW, Dart RL (2011b) The effect of complex fault rupture on the distribution of landslides triggered by the 12 January 2010, Haiti earthquake. Proceedings of the Second World Landslide Forum, Rome: October 3–7, 5 pages
Hovius N, Meunier P, Haines J, Lin CW, Chen H, Dadson S, Horng MJ (2009) Patterns of seismically induced landsliding and the mass balance of a large earthquake. Proceedings of The Next Generation of Research on Earthquake-Induced Landslides, An International Conference in Commemoration of the 10th Anniversary of the Chi-Chi Earthquake, 319–321
Hovius N, Meunier P, Lin CW, Hongey C, Chen YG, Dadson S, Horng MJ, Lines M (2011) Prolonged seismically induced erosion and the mass balance of a large earthquake. Earth Planet Sci Lett 304(3–4):347–355
Huang RQ, Li WL (2009) Analysis of the geo-hazards triggered by the 12 May 2008 Wenchuan earthquake, China. Bull Eng Geol Environ 68(3):363–371
Jibson RW, Harp EL (1994) Landslides triggered by the Northridge earthquake. Earthquakes Volcanoes 25(1):31–41
Jibson RW, Keefer DK (1989) Statistical analysis of factors affecting landslide distribution in the new Madrid seismic zone, Tennessee and Kentucky. Eng Geol 27(1–4):509–542
Kamp U, Growley BJ, Khattak GA, Owen LA (2008) GIS-based landslide susceptibility mapping for the 2005 Kashmir earthquake region. Geomorphology 101(4):631–642
Keefer DK (1984) Landslides caused by earthquakes. Geol Soc Am Bull 95(4):406–421
Keefer DK (2000) Statistical analysis of an earthquake-induced landslide distribution—the 1989 Loma Prieta, California event. Eng Geol 58(3–4):231–249
Keefer DK (2002) Investigating landslides caused by earthquakes—a historical review. Surv Geophys 23(6):473–510
Keefer DK, Wartman J, Ochoa CN, Rodriguez-Marek A, Wieczorek GF (2006) Landslides caused by the M 7.6 Tecomán, Mexico earthquake of January 21, 2003. Eng Geol 86(2–3):183–197
Khazai B, Sitar N (2004) Evaluation of factors controlling earthquake-induced landslides caused by Chi-Chi earthquake and comparison with the Northridge and Loma Prieta events. Eng Geol 71(1–2):79–95
Lee CT, Huang CC, Lee JF, Pan KL, Lin ML, Dong JJ (2008) Statistical approach to earthquake-induced landslide susceptibility. Eng Geol 100(1–2):43–58
Li Z, Chen Q, Zhou JM, Tian BS (2009) Analysis of synthetic aperture radar image characteristics for seismic disasters in the Wenchuan earthquake. J Appl Remote Sens 3(1):031685
Liao HW, Lee CT (2000) Landslides triggered by the Chi-Chi earthquake. ACRS. http://www.a-a-r-s.org/acrs/proceeding/ACRS2000/Papers/HM00-7.htm
Liao C, Liao H, Lee C (2002) Statistical analysis of factors affecting landslides triggered by the 1999 Chi-Chi earthquake, Taiwan. American Geophysical Union, Fall Meeting. http://adsabs.harvard.edu/abs/2002AGUFM.H12D0951L
Lin ML, Tung CC (2004) A GIS-based potential analysis of the landslides induced by the Chi-Chi earthquake. Eng Geol 71(1–2):63–77
Malamud BD, Turcotte DL, Guzzetti F, Reichenbach P (2004a) Landslide inventories and their statistical properties. Earth Surf Process Landf 29(6):687–711
Malamud BD, Turcotte DL, Guzzetti F, Reichenbach P (2004b) Landslides, earthquakes, and erosion. Earth Planet Sci Lett 229(1–2):45–59
Marzorati S, Luzi L, Amicis MD (2002) Rock falls induced by earthquakes: a statistical approach. Soil Dyn Earthq Eng 22(7):565–577
Meunier P, Hovius N, Haines AJ (2007) Regional patterns of earthquake-triggered landslides and their relation to ground motion. Geophys Res Lett 34(20):L20408
Meunier P, Hovius N, Haines AJ (2008) Topographic site effects and the location of earthquake induced landslides. Earth Planet Sci Lett 275(3–4):221–232
Morimoto R (1950) Geology of Imaichi district with special reference to the earthquake of Dec. 26, 1949 (I). Bull Earthq Res Inst 28:379–386
Morimoto R (1951) Geology of Imaichi district with special reference to the earthquake of Dec. 26, 1949 (II). Bull Earthq Res Inst 29:349–358
Morimoto R, Ossaka J, Fukuda T (1957) Geology of Imaichi district with special reference to the earthquake of Dec. 26, 1949 (III). Bull Earthq Res Inst 35:359–375
Morton DM (1971) Seismically triggered landslides above San Fernando Valley. California Geology, Special San Fernando Earthquake Edition, 24(4–5). http://www.johnmartin.com/earthquakes/eqpapers/00000022.htm
Owen LA, Kamp U, Khattak GA, Harp EL, Keefer DK, Bauer MA (2008) Landslides triggered by the 8 October 2005 Kashmir earthquake. Geomorphology 94(1–2):1–9
Parise M, Jibson RW (2000) A seismic landslide susceptibility rating of geologic units based on analysis of characteristics of landslides triggered by the 17 January, 1994 Northridge, California earthquake. Eng Geol 58(3–4):251–270
Parker RN, Densmore AL, Rosser NJ, de Michele M, Li Y, Huang RQ, Whadcoat S, Petley DN (2011) Mass wasting triggered by 2008 Wenchuan earthquake is greater than orogenic growth. Nat Geosci 4(7):449–452
Pearce AJ, O'Loughlin CL (1985) Landsliding during a M 7.7 earthquake: influence of geology and topography. Geology 13(12):855–858
Plafker G, Ericksen GE, Concha FJ (1971) Geological aspects of the May 31, 1970, Peru earthquake. Bull Seismol Soc Am 61(3):543–578
Pradhan B, Youssef AM, Varathrajoo R (2010) Approaches for delineating landslide hazard areas using different training sites in an advanced artificial neural networks model. Geo-Spat Inf Sci 13(2):93–102
Qi SW, Xu Q, Lan HX, Zhang B, Liu JY (2010) Spatial distribution analysis of landslides triggered by 2008.5.12 Wenchuan Earthquake, China. Eng Geol 116(1–2):95–108
Ren ZK, Lin AM (2010) Co-seismic landslides induced by the 2008 Wenchuan magnitude 8.0 earthquake, as revealed by ALOS PRISM and AVNIR2 imagery data. Int J Remote Sens 31(13):3479–3493
Rodriguez CE, Bommer JJ, Chandler RJ (1999) Earthquake-induced landslides: 1980–1997. Soil Dyn Earthq Eng 18(5):325–346
Sato HP, Sekiguchi T, Kojiroi R, Suzuki Y, Iida M (2005) Overlaying landslides distribution on the earthquake source, geological and topographical data: the Mid Niigata prefecture earthquake in 2004, Japan. Landslides 2(2):143–152

Sato HP, Hasegawa H, Fujiwara S, Tobita M, Koarai M, Une H, Iwahashi J (2007) Interpretation of landslide distribution triggered by the 2005 Northern Pakistan earthquake using SPOT 5 imagery. Landslides 4(2):113–122
Sepúlveda SA, Serey A, Lara M, Pavez A, Rebolledo S (2010) Landslides induced by the April 2007 Aysén Fjord earthquake, Chilean Patagonia. Landslides 7(4):483–492
Shen ZK, Sun JB, Zhang PZ, Wan YG, Wang M, Burgmann R, Zeng YH, Gan WJ, Liao H, Wang QL (2009) Slip maxima at fault junctions and rupturing of barriers during the 2008 Wenchuan earthquake. Nat Geosci 2(10):718–724
Tibaldi A, Ferrari L, Pasquare G (1995) Landslides triggered by earthquakes and their relations with faults and mountain slope geometry: an example from Ecuador. Geomorphology 11(3):215–226
US Geological Survey (2008) Shakemap us2008ryan. http://earthquake.usgs.gov/earthquakes/shakemap/global/shake/2008ryan/
Wang WN, Nakamura H, Tsuchiya S, Chen CC (2002) Distributions of landslides triggered by the Chi-chi Earthquake in Central Taiwan on September 21, 1999. Landslides - J Jpn Landslide Soc 38(4):18–26
Wang WN, Wu HL, Nakamura H, Wu SC, Ouyang S, Yu MF (2003) Mass movements caused by recent tectonic activity: the 1999 Chi-chi earthquake in central Taiwan. Island Arc 12(4):325–334
Wang HB, Sassa K, Xu WY (2007) Analysis of a spatial distribution of landslides triggered by the 2004 Chuetsu earthquakes of Niigata Prefecture, Japan. Nat Hazard 41(1):43–60
Wang Q, Qiao XJ, Lan QG, Freymueller J, Yang SM, Xu CJ, Yang YL, You XZ, Tan K, Chen G (2011) Rupture of deep faults in the 2008 Wenchuan earthquake and uplift of the Longmen Shan. Nat Geosci 4(9):634–640
Wasowski J, Gaudio VD, Pierri P, Capolongo D (2002) Factors controlling seismic susceptibility of the Sele Valley slopes: the case of the 1980 Irpinia earthquake re-examined. Surv Geophys 23(6):563–593
Wasowski J, Keefer DK, Lee CT (2011) Toward the next generation of research on earthquake-induced landslides: current issues and future challenges. Eng Geol 122(1–2):1–8
Weiss AD (2006) Topographic position and landforms analysis. http://www.jennessent.com/downloads/tpi-poster-tnc_18x22.pdf
Weissel JK, Stark CP (2001) Landslides triggered by the 1999 Mw7.6 Chi Chi earthquake in Taiwan and their relationship to topography. Geoscience and Remote Sensing Symposium, 2001. IGARSS '01. IEEE 2001 International 2: 759–761
Xu C, Xu XW (2012a) Spatial distribution of seismic landslides and their erosion thickness relate with a transpressional fault caused earthquake of subduction zone. J Eng Geol 20(5):732–744 (in Chinese)
Xu C, Xu XW (2012b) Comment on "Spatial distribution analysis of landslides triggered by 2008.5.12 Wenchuan Earthquake, China" by Shengwen Qi, Qiang Xu, Hengxing Lan, Bing Zhang, Jianyou Liu [Engineering Geology 116 (2010) 95–108]. Engineering Geology 133–134: 40–42
Xu C, Xu XW (2012c) Spatial prediction models for seismic landslides based on support vector machine and varied kernel functions: a case study of the 14 April 2010 Yushu earthquake in China. Chin J Geophys 55(6):666–679
Xu C, Xu XW (2013) Controlling parameter analyses and hazard mapping for earthquake triggered-landslides: an example from a square region in Beichuan County, Sichuan Province, China. Arab J Geosci. doi:10.1007/s12517-012-0646-y
Xu ZQ, Ji SC, Li HB, Hou LW, Fu XF, Cai ZH (2008a) Uplift of the Longmen Shan range and the Wenchuan earthquake. Episodes 31(3):291–301
Xu XW, Wen XZ, Ye JQ, Ma BQ, Chen J, Zhou RJ, He HL, Tian QJ, He YL, Wang ZC, Sun ZM, Feng XJ, Yu GH, Chen LC, Chen GH, Yu SE, Ran YK, Li XG, Li CX, An YF (2008b) The Ms 8.0 Wenchuan earthquake surface ruptures and its seismogenic structure. Seismol Geol 30(3):597–629 (in Chinese)
Xu C, Dai FC, Chen J, Tu XB, Xu L, Li WC, Tian W, Cao YB, Yao X (2009a) Identification and analysis of secondary geological hazards triggered by a magnitude 8.0 Wenchuan earthquake. J Remote Sens 13(4):745–762 (in Chinese)
Xu XW, Wen XZ, Yu GH, Chen GH, Klinger Y, Hubbard J, Shaw J (2009b) Coseismic reverse- and oblique-slip surface faulting generated by the 2008 Mw 7.9 Wenchuan earthquake, China. Geology 37(6):515–518
Xu XW, Yu GH, Chen GH, Ran YK, Li CX, Chen YG, Chang CP (2009c) Parameters of coseismic reverse- and oblique-slip surface ruptures of the 2008 Wenchuan earthquake, eastern Tibetan plateau. Acta Geol Sin 83(4):673–684
Xu C, Xu XW, Yu GH (2012a) Study on the characteristics, mechanism, and spatial distribution of Yushu earthquake triggered landslides. Seismol Geol 34(1):47–62 (in Chinese)
Xu C, Xu XW, Yu GH (2012b) Earthquake triggered landslide hazard mapping and validation related with the 2010 Port-au-Prince, Haiti earthquake. Disaster Adv 5(4):1297–1304
Xu C, Dai FC, Xu XW, Lee YH (2012c) GIS-based support vector machine modeling of earthquake-triggered landslide susceptibility in the Jianjiang River watershed, China. Geomorphology 145–146:70–80
Xu C, Xu XW, Dai FC, Saraf AK (2012d) Comparison of different models for susceptibility mapping of earthquake triggered landslides related with the 2008 Wenchuan earthquake in China. Comput Geosci 46:317–329
Xu C, Xu XW, Lee YH, Tan XB, Yu GH, Dai FC (2012e) The 2010 Yushu earthquake triggered landslide hazard mapping using GIS and weight of evidence modeling. Environ Earth Sci 66(6):1603–1616
Xu C, Xu XW, Dai FC, Xiao JZ, Tan XB, Yuan RM (2012f) Landslide hazard mapping using GIS and weight of evidence model in Qingshui river watershed of 2008 Wenchuan earthquake struck region. J Earth Sci 23(1):97–120
Xu C, Xu XW, Yu GH (2013a) Landslides triggered by slipping-fault-generated earthquake on a plateau: an example of the 14 April 2010, Ms 7.1, Yushu, China earthquake. Landslides. doi:10.1007/s10346-012-0340-x
Xu C, Xu XW, Yao Q, Wang YY (2013b) GIS-based bivariate statistical modeling for earthquake-triggered landslides susceptibility mapping related to the 2008 Wenchuan earthquake, China. Q J Eng Geol Hydrogeol. doi:10.1144/qjegh2012-006
Xu C, Xu XW, Dai FC, Wu ZD, He HL, Wu XY, Xu SN, Shi F (2013c) Application of an incomplete landslide inventory, logistic regression model and its validation for landslide susceptibility mapping related to the May 12, 2008 Wenchuan earthquake of China. Nat Hazards. doi:10.1007/s11069-013-0661-7
Yagi H, Higaki D, Yamamoto M, Yamasaki T (2009) Distribution and characteristics of landslides induced by the Iwate–Miyagi Nairiku earthquake in 2008 in Tohoku District, Northeast Japan. Landslides 6(4):335–344
Yalcin A (2008) GIS-based landslide susceptibility mapping using analytical hierarchy process and bivariate statistics in Ardesen (Turkey): comparisons of results and confirmations. Catena 72(1):1–12
Yamagishi H, Iwahashi J (2007) Comparison between the two triggered landslides in Mid-Niigata, Japan by July 13 heavy rainfall and October 23 intensive earthquakes in 2004. Landslides 4(4):389–397
Yin JH, Chen J, Xu XW, Wang XL, Zheng YG (2010a) The characteristics of the landslides triggered by the Wenchuan Ms 8.0 earthquake from Anxian to Beichuan. J Asian Earth Sci 37(5–6):452–459
Yin YP, Zhang YS, Ma YS, Hu DG, Zhang ZC (2010b) Research on major characteristics of geohazards induced by the Yushu Ms7.1 earthquake. J Eng Geol 18(3):289–296 (in Chinese)
Zhang WJ, Lin JY, Peng J, Lu QF (2010) Estimating Wenchuan earthquake induced landslides based on remote sensing. Int J Remote Sens 31(13):3495–3508

C. Xu · X. Xu
Key Laboratory of Active Tectonics and Volcano,
China Earthquake Administration,
Beijing 100029, People's Republic of China

C. Xu (✉) · X. Xu
Institute of Geology,
China Earthquake Administration,
Beijing 100029, People's Republic of China
e-mail: xc11111111@126.com

X. Yao
Institute of Geomechanics,
Chinese Academy of Geological Sciences,
Beijing 100081, People's Republic of China

F. Dai
Institute of Geology and Geophysics,
Chinese Academy of Sciences,
Beijing 100029, People's Republic of China